NASA Technical Memorandum 78800

Description and Preliminary Calibration Results for the Langley Hypersonic CF_4 Tunnel

R. E. Midden and C. G. Miller

November 1978

National Aeronautics and Space Administration

Langley Research Center
Hampton, Virginia 23665

SUMMARY

A detailed description of the Langley hypersonic CF_4 tunnel is presented along with discussion of the basic components, instrumentation, and operating procedure. Operational experience with the CF_4 reclaimer and lead-bath heater is discussed.

Pitot pressure surveys were measured at the nozzle exit and downstream of the exit for nominal reservoir temperatures of 608 K, 717 K, and 815 K and range of reservoir pressure from 6.9 to 17.3 MN/m^2. At the maximum value of reservoir pressure and temperature, which corresponds to the reservoir conditions for which the contoured axisymmetric nozzle was designed, a uniform test core having a diameter of approximately 28 cm (0.55 times the nozzle exit diameter) exists. The corresponding free stream Mach number is 5.9, unit Reynolds number is 1.2×10^6 per meter, ratio of specific heats is 1.17, and the normal shock density ratio is equal to 12.6. When the facility is operated at reservoir pressures and temperatures below the design values, "dips" and "spikes" occur on the centerline pitot pressure, indicating the existence of flow disturbances originating in the upstream region of the nozzle. These "dips" and "spikes" are relatively small in magnitude, and in general, result in a perturbation in centerline free stream Mach number of less than 1 percent. The development of a saddle-like pitot pressure distribution (toroid of high pitot pressure that surrounds an inner core of uniform pitot pressure) with increasing distance downstream of the exit was observed. A slight decrease in average pitot pressure across the test core with distance downstream of the nozzle was observed, with the corresponding free stream Mach number variation being about 0.3 percent for a distance of 20.3 cm. Comparison of measured and predicted shock detachment distance on a sphere and pressure distributions measured on a sharp leading-edge flat plate revealed the absence of significant flow nonuniformity and lent creditability to predicted free stream flow conditions.

The economic operation of this facility centers about the CF_4 reclaimer, which was designed to operate at an efficiency of 90 to 95 percent. A number of modifications have been made to the reclaimer system to improve its performance, and presently, the system reclaims approximately 75 percent of the test gas. Even with current budgetary constraints, this efficiency permits the CF_4 tunnel to be operated as a viable research wind tunnel.

INTRODUCTION

During entry of blunt vehicles into Earth and planetary atmospheres, values of normal-shock density ratio are encountered which are significantly larger than values generated in conventional-type hypersonic air wind tunnels. These high values of density ratio result from the excitation of vibration, dissociation and ionization energy modes of the atmospheric gas passing

through the bow shock about the vehicle. As dissociation is initiated, the temperature within the shock layer decreases as energy is absorbed in exciting vibrational levels and dissociating molecules, the static pressure increases only slightly, hence, the density experiences a much larger increase in comparison to the ideal-gas value. These phenomena are commonly referred to as real-gas effects.

The importance of real-gas effects has been recognized for over 2 decades, since the primary factor governing the inviscid flow field about blunt bodies at hypersonic speeds is the normal shock density ratio. For example, the bow shock detachment distance is dependent on the density ratio across the shock and is of practical importance in radiative heat transfer studies because it determines the volume of gas available to radiate. Also, real-gas effects may be significant in the analysis of aerodynamic characteristics because of changes in the level of surface pressure and the pressure distribution over the surface of the vehicle.

Unfortunately, the majority of data demonstrating real-gas effects are analytical, and little experimental data exist upon which to verify the various computer codes. This relative scarcity of experimental data at high values of normal-shock density ratio is due, in part, to development and hardware problems associated with high-enthalpy facilities capable of generating hypersonic, real-gas flows. Most such facilities are impulse-type or a ballistic range. The disadvantages of such facilities, as compared to ideal-gas conventional-type wind tunnels, are well recognized. (Examples of disadvantages are short test times, poor test repeatability, flow contamination, complex instrumentation with associated poor reliability and relatively large uncertainties, and departure from equilibrium flow during the nozzle expansion process or within the shock layer of the test model.) An alternate method for generating high density ratio at hypersonic conditions, but low enthalpies, is to employ a test gas characterized by a low ratio of specific heats in a conventional-type wind tunnel. A study of this method is reported in reference 1, where CF_4 was used as the test gas in a small pilot model wind tunnel having a 5° half-angle conical nozzle and 7.6-cm diameter test section. CF_4 was selected (ref. 1) because of its low ratio of specific heats, low boiling point, thermal stability, and low vibrational relaxation time, and because it is readily available, colorless, odorless, nontoxic, and should be easily reclaimed. These tests with CF_4 demonstrated that values of density ratio as high as 12 were obtained at a free stream Mach number of 6, and measured pitot pressure and nozzle wall (free stream static) pressure were in good agreement with prediction. They also demonstrated the desirability of having a larger CF_4 wind tunnel; hence, the Langley 20-inch hypersonic arc-heated tunnel (ref. 2) was converted to the Langley hypersonic CF_4 tunnel. When this facility is used in conjunction with the Langley 20-inch Mach 6 air wind tunnel, density ratios of approximately 5.5 and 12 are provided at a Mach number of 6. This range of density ratio should provide valuable simulation of real-gas effects.

The primary purpose of this report is twofold. First, a general description of the Langley hypersonic CF_4 tunnel along with a discussion of operational experience is presented. Second, the results from pitot pressure

surveys (radially and axially) measured at the test section for a range of reservoir supply pressure and temperature are presented, along with limited results from hemisphere-cylinder models and a sharp leading-edge flat plate.

SYMBOLS

L	distance along surface centerline of flat plate from leading edge, m
M	Mach number
N_{Pr}	Prandtl number
N_{Re}	unit Reynolds number, m^{-1}
p	pressure, N/m^2
$\dot{q}$	heat transfer rate, W/m^2
r	radius, m
t	time, sec
T	temperature, K
x,y,z	nozzle or model coordinates (rectangular coordinates where x is the horizontal axis, y is the vertical axis, and z is along the nozzle axis, with z = 0 at nozzle exit, m
Z	compressibility factor
γ	ratio of specific heats
μ	viscosity, $N\text{-}sec/m^2$
ρ	density, kg/m^3
θ	angle subtended by a circular arc measured from the sphere axis of symmetry through the stagnation point, deg

Subscripts:

avg	average value
CL	nozzle centerline
e	nozzle exit
n	model nose
w	wall
t,1	reservoir stagnation conditions

t,2 stagnation conditions behind normal shock

∞ free stream static conditions

2 static conditions behind normal shock

Superscript:

Barred symbol denotes average or mean value

FACILITY

The Langley hypersonic CF_4 tunnel is a conventional-type, blow-down wind tunnel that uses tetrafluoromethane (CF_4) as the test gas. This facility, which represents a conversion of the Langley 20-inch hypersonic arc-heated tunnel (ref. 2) to the present mode, is shown schematically and photographically in figure 1. Basic components include a high-pressure storage field, pressure regulator, lead-bath heaters, nozzle, test section, diffuser, vacuum system, and CF_4 reclaimer. These basic components will now be discussed briefly.

High-pressure system.- This system consists of a compressor capable of producing pressures up to 34.5 MN/m^2, storage bottles, storage trailer, pressure regulator and applicable control valves. The bottle field consists of two groups of three storage bottles, with each bottle having a volume of 0.85 m^3 and a design pressure of 34.5 MN/m^2. The storage bottles are generally maintained at pressures between 17 and 24 MN/m^2 and are located external to the building that houses the test section; hence, they are at outside ambient temperature. The supply trailer is rated for a maximum pressure of 17 MN/m^2. The desired pressure or mass flow of CF_4 from the storage bottles into the heaters is controlled by a Powreactor pressure regulator.

Heaters.- The CF_4 test gas is heated to a maximum temperature of approximately 900 K by two lead-bath heaters in parallel. A sketch of the heater is shown in figure 2. Each heater contains 9.1 Mg of molten lead which is heated by 18 heating elements, each rated at 4 kW. The test gas flows through 44 spirally wound stainless steel tubes, having an inside diameter of 7 mm and outside diameter of 9.5 mm, immersed in the molten lead container. The maximum design pressure for the heater is 24 MN/m^2. The 440 volt resistance heaters that heat the molten lead are controlled thermostatically. Each heater requires approximately 6 hours to achieve an equilibrium temperature from the ambient temperature, and has a 45-minute recovery time for a 310 K drop in temperature. The flow rate through the heater ranges from approximately 1 to 4 kg/sec.

Settling chamber and nozzle.- The settling chamber is a pressure vessel that is 30.5 cm long and has an inside diameter of 17.8 cm. The tubing between the heaters and settling chamber as well as the settling chamber itself are wrapped with electric resistance heaters to minimize heat loss from the CF_4 test gas as it travels from the heater to the nozzle. This tubing, settling chamber, and nozzle throat region are wrapped with insulation. The nozzle is axisymmetric and contoured, with a nozzle throat diameter of 1.07 cm and nozzle exit diameter of 50.8 cm. This nozzle was designed using the method of

references 1 and 3 to generate Mach 6 flow in CF_4 at the nozzle exit for a stagnation pressure equal to 17.6 MN/m^2 and stagnation temperature equal to 811 K. The settling chamber and stainless steel nozzle are designed for a maximum pressure of 34.5 MN/m^2.

Test section.- The flow exhausts from the nozzle into a tank approximately 1.8 m long and with an internal diameter of 1.5 m; hence, models are tested in an open jet. Models are supported at the nozzle exit by a pneumatically driven insert mechanism designed on the circular arc principle with the center of rotation fixed on the nozzle centerline. The angle of attack may be varied over a range of ±20°, with a 0.1° uncertainty. The injection time (time required for model to move from prerun position to nozzle centerline) is approximately 1 second and retraction time approximately 2 seconds. The test section tank is protected from overpressure by a dead weight relief valve designed to open at 170 kN/m^2. Schlieren quality windows measuring 61 × 76 cm are located on opposite sides of the tank for flow visualization purposes.

Vacuum system.- Having exited the nozzle and passed over the test model, the test gas is collected by a diffuser and passed through a water-cooled heat exchanger to reduce the gas temperature. The gas is then dumped into two vacuum spheres. The vacuum spheres have diameters of 5.2 m and 15.5 m for a combined total volume of 2023 m^3. The spheres are evacuated to a pressure of approximately 35 N/m^2 by three vacuum pump-blower combinations. A fourth vacuum pump-blower combination is used to evacuate the nozzle and test section to approximately 35 N/m^2 prior to a run.

Reclaimer.- The CF_4 reclaimer is an extremely important component of the CF_4 tunnel. Because of the large mass flow rates of this facility in comparison to the pilot model CF_4 tunnel and the present cost of CF_4 of approximately $25 per kg, a reclaimer is necessary for economical operation. A schematic drawing of the reclaimer is shown in figure 3. As mentioned previously, the vacuum spheres serve as receivers for the CF_4 test gas. Having collected CF_4 from a single run or several runs, the spheres are evacuated with the exhaust of the vacuum pumps supplying CF_4 to the reclaimer. The contaminated CF_4 gas first passes through a heat exchanger to initially cool it, then through a separator (filter) for oil and water removal, then through a second heat exchanger. The gas next travels into a liquid nitrogen cooled condenser. In this reservoir (fig. 3), the CF_4 is liquefied and the gaseous impurities are exhausted to atmosphere. The nominal operating pressure of this reservoir is 1.3 MN/m^2. The liquid CF_4 is compressed to approximately 34.5 MN/m^2 by a liquid pump and this compressed liquid passed through a vaporizer to convert it to a gaseous state. The high-pressure gaseous CF_4 is then stored in the storage bottles. Liquid nitrogen is supplied to the reservoir (condenser) from a 4000-gallon liquid nitrogen trailer maintained at a pressure of 270 kN/m^2.

Operating Procedure

To prepare the facility for a run, the settling chamber, nozzle, test section, diffuser, and vacuum spheres are evacuated to a pressure of about 35 N/m^2. The lead-bath heaters are brought to the desired stagnation

temperature for the CF_4 test gas, and the pressure regulator set to the desired stagnation pressure. Appropriate valves are opened by a timer and flow is established in the nozzle. Following the establishment of steady flow, the test model is injected into the flow at a preset time (usually about 2 seconds after nozzle flow establishment), and retracted just prior to tunnel shutdown. Usage of both vacuum spheres provides a maximum run time of approximately 45 seconds. Tunnel shutdown is accomplished by closing the main isolation valve. Because of the relatively large volume of the spheres, a number of short duration runs may be performed before the spheres must be evacuated. Having completed the desired test(s), the contents of the spheres are exhausted into the CF_4 reclaimer. To minimize impurities in the CF_4, the spheres are emptied immediately after a run series into the reclaimer, and the CF_4 test gas not allowed to remain in the spheres overnight. In an effort to further reduce impurities, the facility is maintained under vacuum and opened to the atmosphere only when necessary (for example, to perform model change.)

Instrumentation

Quantities measured routinely for each run are stagnation pressure $p_{t,1}$ and stagnation temperature $T_{t,1}$ in the settling chamber and pitot pressure $p_{t,2}$ just downstream of the nozzle exit. The stagnation pressure is measured with a strain-gage pressure transducer having a full-scale rating of 21 MN/m^2. This transducer, which is calibrated periodically over the range 0 to 21 MN/m^2, is believed to provide values of $p_{t,1}$ accurate to within 2 percent. Stagnation temperature is measured with a chromel-alumel shielded thermocouple inserted through the wall of the settling chamber and positioned in the center of the chamber. Measured values of $T_{t,1}$ are believed accurate to within 3 to 5 percent. Pitot pressure is generally measured with a flat-faced cylindrical probe having an inside diameter of 1.5 mm and outside diameter of 2.3 mm. Either a variable capacitance diaphragm transducer or a strain-gage pressure transducer is used to monitor the pitot pressure during a run. This measurement is believed to be accurate to within 2 percent.

Basic measurements performed with test models include forces and moments, surface pressure, surface heat transfer rate, and shock shapes. A total of 45 channels of pressure instrumentation exists, of which three to five channels are used to monitor facility performance. Of these 45 channels, 10 employ variable capacitance transducers and the remaining channels employ strain-gage pressure transducers. Surface heat transfer rates are generally measured using the thin skin calorimeter technique; that is, the heat transfer rate is inferred from the temperature-time history supplied by a thermocouple welded onto the inside surface of the model shell. For this technique, the model is injected into the flow for a short period of time, usually 2 to 3 seconds. A limiting switch indicates the time at which the model has reached the center of the nozzle. Presently, 42 channels are available for chromel-alumel thermocouples. A hot (339 K) junction box is employed. The output from pressure transducers, thermocouples, and force balance are recorded on a magnetic tape having a sampling rate of 400 samples per second for each channel.

Shock shapes are measured with the dual plate holographic interferometer system shown schematically in figure 4 and discussed in detail in reference 4. Holograms were recorded using a pulsed ruby laser that provided a 50 mj pulse of 20 ns duration. A 6 mw He-Ne alignment laser was positioned behind the ruby laser and a third laser (50 mw He-Ne) is used for reconstruction. The holograms obtained may be used to produce shadowgraphs, schlieren photographs, or interferograms of the test flow. A representative interferogram is illustrated in figure 5 for a parabolic, axisymmetric model at zero angle of attack.

Survey Rake

Pitot pressure surveys at the nozzle exit and downstream of the exit were measured with a cross-pattern rake having 19 pitot probes (including the center probe) positioned vertically and 12 pitot probes positioned horizontally. The center probe was coincident with the nozzle centerline. With the exception of the five centermost probes, the probes were spaced 2.54 cm apart; the five center probes were spaced 1.27 cm apart. Hence, the 31-probe rake covered a vertical distance 21.6 cm above and below the nozzle centerline and horizontal distance of 14 cm to either side of the centerline. Pitot probes were flat-faced tubes having an inside diameter of 1.5 mm and length of 2.54 cm.

PREDICTED FLOW PROPERTIES

Free stream and behind the normal shock thermodynamic and transport properties were determined from the procedure discussed in references 1 and 5. Basic inputs are measured reservoir stagnation pressure $p_{t,1}$, stagnation temperature $T_{t,1}$, and pitot pressure $p_{t,2}$. From the measured stagnation pressure and stagnation temperature, the corresponding value of density is obtained using the imperfect (intermolecular force effects are accounted for) equation of state. The entropy is determined from the temperature and density and an isentropic, one-dimensional expansion performed. Thermodynamic equilibrium is assumed throughout the flow process; hence, possible effects of vibrational nonequilibrium are not included. Justification for not including vibrational relaxation effects in the methods of references 1 and 5 is discussed in reference 1. The flow is expanded to a given value of free stream temperature and the remaining free stream thermodynamic properties of interest are obtained from the isentropic condition and equations presented in references 1 and 5. The free stream velocity, hence Mach number, is determined from the conservation of energy, and the usual normal shock relations are employed to obtain static conditions immediately behind the shock. Stagnation conditions behind the shock are obtained by bringing the flow to rest isentropically and from consideration of the conservation of energy. Values of free stream temperature are tried until the calculated stagnation point (pitot) pressure agrees with the measured pitot pressure. For the range of reservoir stagnation conditions of this study, the compressibility factor, which represents the degree of departure from ideal-gas behavior, varied from approximately 1.03 to 1.12. Imperfect gas effects at the free stream conditions and behind the normal shock are essentially negligible (that is, the

compressibility factor is unity). The equations used in references 1 and 5 are limited to temperatures above the saturated vapor line. For the range of conditions of this study, flow condensation effects should be absent.

Monitoring the mass of CF_4 within the high pressure storage bottles before and after a test or series of tests provides a measure of the efficiency of the reclaimer system. The mass is deduced from the measured bottle-field pressure and ambient (outdoor) temperature. As shown in figure 6, where the compressibility factor (refs. 1 and 5) is plotted as a function of pressure for various temperatures, a significant departure from ideal-CF_4 behavior occurs for the nominal bottle-field pressure of 20 MN/m^2 and temperature range of 275 K to 310 K. The results of figure 6 demonstrate the importance of accounting for intermolecular force effects in the determination of reclaimer efficiency and the quantity of CF_4 available for testing.

TESTS

Tests with the pitot pressure survey rake were performed for a range of settling chamber pressure and temperature. Three values of stagnation temperature $T_{t,1}$ were tested, the mean values being 608 K, 717 K, and 815 K. For each value of $T_{t,1}$, three values of stagnation pressure $p_{t,1}$ were tested, these values being 6.9, 12.1, and 17.6 MN/m^2. The survey rake was positioned with the longest cross-member vertical and the rake was moved axially such that the sensing surface of the probes were positioned at the nozzle exit and 10.2, 20.3, and 30.5 cm downstream of the exit. Predicted flow quantities (p_∞, T_∞, M_∞, $N_{Re,\infty}$, ρ_2/ρ_∞, and $N_{Re,2}$) corresponding to the various combinations of measured $p_{t,1}$, $T_{t,1}$, and $\bar{p}_{t,2}$ are presented in table I. The input value of $\bar{p}_{t,2}$ represents an average of the measured pitot pressure across the inviscid test core, excluding the center probe for reasons to be discussed subsequently. Samples of the collected test gas were analyzed periodically for purity. For the present tests, the CF_4 test gas was at least 99.9 percent pure.

OPERATING EXPERIENCE

As expected in such an undertaking, a number of problems were encountered in the conversion of the Langley 20-inch hypersonic arc-heated tunnel to the hypersonic CF_4 tunnel. Two such problems unique to CF_4 operation will be discussed.

During the shakedown of the facility, an unexpected decrease in performance occurred during a sequence of tests. The source of this problem was traced to blockage of the stainless steel screen located within the settling chamber. As shown in the photograph of figure 7, the blockage resulted from a collection of rust-like particles by the screen. Now, the tubing from the high-pressure storage field and through the lead-bath heaters is AISI 316 stainless steel and pure CF_4 will not corrode this tubing material. However, CF_4 contaminated with water vapor or oil will react at the present conditions to form HF, which will corrode AISI 316 stainless steel. Spectrochemical analysis of contaminants taken from the inside of a section of tube removed from the lead-bath heater revealed the tubing was corroding and this corrosion resulted in

the blockage of the screen. A source of water vapor into the supply line was discovered and eliminated. Previous to this blockage of the screen, a diaphragm in the CF_4 compressor ruptured allowing oil to enter the tubing; hence, an oil detector was installed in the supply line to provide an immediate warning of the presence of oil. With the sources of water vapor or oil eliminated, the screen was removed from the settling chamber and testing resumed. Models tested following these changes indicated a slight sandblasting effect. The present level of flow contamination is not expected to significantly influence pressure or force and moment measurements on models, and the effect on heat transfer measurements is negligible, as will be shown subsequently. This corrosion of the tube wall did not reduce the wall thickness below acceptable limits for the safe operation of the facility.

The CF_4 reclaimer was designed and manufactured specifically for the CF_4 tunnel. At the time of fabrication, no data base for such a system was available to the manufacturer. Thus, it is not surprising that several problems were encountered during the initial operation of this reclaimer.

The reclaimer was installed into the vacuum system employed with the Langley 20-inch hypersonic arc-heated tunnel. Initial operation with the reclaimer revealed a blockage problem, attributed to water and oil contaminants solidifying in the primary heat exchanger and condenser (fig. 3), thereby blocking the line. These solid particles entered the liquid pump, resulting in damaged intake and exhaust valves. Although a small molecular sieve filter preceded the primary heat exchanger, the water and oil contaminants still found their way to the condenser and liquid pump. The primary source of water is from the air within the facility and water vapor contained within the walls of the nozzle, dump tank, and diffuser. To avoid subjecting the reclaimer to this water, a separate vacuum pump was used to evacuate the facility. The exhaust system of the vacuum pumps used to evacuate the spheres (fig. 1) was not designed for low vacuums and contained a number of leaks. Leak checks were performed to locate and correct these leaks, thereby minimizing another source of water vapor. Also, the exhaust system was evacuated prior to a reclaiming cycle. The source of oil is the vacuum pumps. A small booster pump, which increased the reclaimer pressure from approximately 0.5 to 1.5 kN/m^2 to 3.5 to 4.5 kN/m^2, was removed as a potential source of contaminants. No adverse effect on system performance was observed due to the decrease in operating pressure. The filter capability was improved by installing two large filters ahead of the primary heat exchanger, one filter filled with vaporsurb and the other with activated charcoal. The first heat exchanger was changed from water cooling to LN_2 cooling, and thus served as a cold trap. In addition, the heat exchangers were wrapped with resistance heaters so they could be dried out between reclaimer cycles. These modifications eliminated the blockage problem and greatly reduced the water and oil contamination level at the condenser.

During the shakedown, the reclaimer demonstrated an intermittent behavior. For some reclaiming cycles, most of the CF_4 gas appeared to have been reclaimed, whereas for other cycles, none was reclaimed. This behavior was traced to a faulty vent valve and led to the replacement of butterfly valves with gate valves wherever practical. Presently, the reclaimer operates smoothly, free of

hardware problems, at an efficiency of 70 to 75 percent, compared to the manufacturer's design efficiency of 90 to 95 percent. This efficiency is expected to increase to about 80 to 85 percent when the volume of the exhaust line is reduced and provision made to reclaim the CF_4 gas in this line following a reclaiming cycle. Analysis of the waste gas from the condenser showed that only 1 percent of the gas was CF_4. Thus, a realistic efficiency for the present reclaimer system appears to be 80 to 85 percent, and this efficiency is sufficient for continuous, economical operation of the facility.

RESULTS AND DISCUSSION

Facility calibration consisted primarily of pitot pressure surveys with a 31-probe survey rake which covered a vertical distance 21.6 cm above and below the nozzle centerline and horizontal distance of 14 cm to either side of the centerline. The inviscid test core diameter was defined as the region in which the pitot pressure was within 2 percent of the average value of the center 13 vertical probes, excluding the centerline pitot pressure. For the present conditions, a 2-percent uncertainty in the pitot pressure corresponds to a 0.2 to 0.25-percent uncertainty in free stream Mach number.

To optimize the usage of the CF_4 test gas, the facility run duration is generally tailored to the type of measurement to be performed. Representative time histories of reservoir stagnation pressure, stagnation temperature, and corresponding pitot pressure are shown in figure 8. A time of zero corresponds to the first data sample indicating an increase in pitot pressure from the prerun (quiescent test section) value. The time histories of figure 8 demonstrate that approximately 3.5 seconds are required to establish a steady flow condition, and the duration of this steady flow for this case is approximately 5 seconds. The present values of pitot pressure measured with the survey rake correspond to a test time of 6 to 8 seconds and thus represent steady flow values. This flow duration is also satisfactory for heat transfer tests using the thin-skin calorimeter technique. However, the run duration must be increased for studies involving the measurement of pressures on the order of the free stream static pressure. For example, time histories of the nozzle wall pressure measured 1.27 cm and 30.48 cm upstream of the nozzle exit are shown in figure 9. Because of the low level of nozzle wall pressure, a pressure lag effect exists for the present pressure measuring system and approximately 22 to 24 seconds are required to obtain a steady value of wall pressure 30.48 cm upstream of the nozzle exit. This steady value of nozzle wall pressure is within 2 percent of the calculated free stream static pressure, which corresponds to the pitot pressure measured at the nozzle exit. The rather sharp increase in nozzle wall pressure 1.27 cm upstream of the exit at a time of 7 seconds, or so, is believed to be due to an increase in the test section (dump tank) pressure, from the quiescent ($t < 0$) value of 70 N/m^2, with run time. This pressure increase is fed upstream through the nozzle boundary layer, but the adverse pressure gradient is sufficiently weak so to not disturb the boundary layer 30.48 cm upstream of the nozzle exit.

Pitot pressure surveys for a nominal reservoir temperature $T_{t,1}$ of 608 K (±4 percent) and range of reservoir pressure are shown in figures 10, 11, and 12 for nozzle axial stations z equal to 0 (nozzle exit), 10.2 and

20.3 cm downstream of the exit. At the nozzle exit (fig. 10) and 20.3 cm downstream of the exit (fig. 12), the measured centerline pitot pressure is significantly lower than the adjacent pitot pressures. At an axial station of 10.2 cm, the centerline pitot pressure is higher than adjacent pitot pressures. The data of figure 10 for $z = 0$ indicate this "dip" or decrease in centerline pitot pressure may diminish with increasing reservoir pressure $p_{t,1}$, whereas the "spike" or increase in centerline pitot pressure observed at $z = 10.2$ cm (fig. 11) becomes more pronounced as $p_{t,1}$ is increased. The observance of a "dip" or "spike" on centerline pitot pressure implies a flow disturbance exists in the upstream region of the nozzle, resulting in a focusing effect of disturbances along the nozzle centerline. The observed "dips" and "spikes" are believed to be characteristic of the flow, and not attributed to probe interference effects due to the closer probe spacing about the center probe or to a faulty pressure transducer.

Reasonably flat and symmetrical (about the nozzle centerline) pitot pressure profiles were obtained across a 28 cm to 38 cm diameter inviscid core for all values of reservoir pressure and axial station. At axial stations of 10.2 cm and 20.3 cm, there is some indication of the formation of a saddle-like distribution, whereby a region of higher pitot pressure surrounds an inner, uniform pitot pressure region. From figures 10, 11, and 12, no appreciable variation of pitot pressure ratio is observed between axial stations z equal to 0 and 20.3 cm, implying the absence of significant source-flow effects.

Pitot pressure surveys for a nominal reservoir temperature of 717 K (±2.5 percent) are shown in figures 13 to 18 for the same range of reservoir pressure as in figures 10 to 12, and various nozzle axial stations from 0 to 30.5 cm downstream of the nozzle exit. As observed for $\bar{T}_{t,1}$ equal to 608 K (figs. 10, 11, and 12), the pitot pressure profiles generally exhibit a "dip" or "spike" on the nozzle centerline. For $\bar{T}_{t,1}$ equal to 717 K, a pronounced spike in centerline pitot pressure is observed at the nozzle exit (fig. 13), whereas a dip in centerline pitot pressure was observed at the nozzle exit for $\bar{T}_{t,1}$ equal to 608 K (fig. 10). Assuming, of course, that the centerline pitot pressure is measured accurately (within 2 percent), the variation in the character (dip or spike) of the centerline pitot pressure with change in reservoir temperature is attributed to the effect of reservoir temperature on the nozzle boundary layer displacement thickness. The pitot pressure survey 2.5 cm downstream of the exit reveals a "dip" in centerline pitot pressure, whereas that at z equal to 5.1 cm illustrates a possible change of a "dip" condition to a "spike" condition with increasing reservoir pressure, although experimental uncertainty prohibits a definite conclusion. In general, the "dip" condition is observed for values of z exceeding 5.1 cm.

As observed previously, the pitot pressure profiles exhibit a symmetrical saddle-like characteristic about the nozzle centerline. This saddle-like feature becomes more pronounced with increasing distance from the nozzle exit and is attributed to disturbances (weak waves) embedded within the flow due to the expansion process at the nozzle exit. The results of figures 13 to 18 demonstrate that the inviscid test core diameter is approximately 28 cm for the range of z tested. Because of the nature of the pitot pressure

profiles for $\bar{T}_{t,1}$ equal to 717 K, models tested at these conditions will not be subjected to uniform flow and measurements performed with such models, particularly slender ones, may be subject to question.

Pressure surveys for a nominal reservoir temperature of 815 K (±3 percent) and range of reservoir pressure are shown in figures 19, 20, and 21 for values of z equal to 0, 10.2, and 20.3 cm. Unlike the previous results for $\bar{T}_{t,1}$ equal to 608 K and 717 K, these profiles (figs. 19 to 21) do not exhibit a "dip" or "spike" in centerline pitot pressure at the higher values of reservoir pressure. The flow about the nozzle axis is relatively uniform at z equal to 10.2 cm and 20.3 cm for all values of $p_{t,1}$ and a pronounced "dip" is observed only at the nozzle exit for the lowest value of $p_{t,1}$ (fig. 19(a)). Again, the pitot-pressure surveys illustrate a saddle-like characteristic which becomes more pronounced with increasing z. From the various combinations of reservoir pressure and temperature, the most uniform pitot pressure distribution between the nozzle exit and 20.3 cm downstream of the exit is achieved with a reservoir temperature of approximately 815 K and pressure of approximately 17.6 MN/m^2. That is, the absence of irregularities in pitot pressure distributions were observed only for reservoir conditions close to those used in the design of the nozzle.

The average pitot pressure ratio $\bar{p}_{t,2}/p_{t,1}$ across the inviscid test core is shown in figure 22 as a function of stagnation pressure $p_{t,1}$ for the three values of nominal stagnation temperature $T_{t,1}$. Within the experimental accuracy (denoted by barred symbols), the pitot pressure ratio measured at the nozzle exit is essentially independent of stagnation pressure for the range of reservoir conditions examined. For a given stagnation pressure, the pitot pressure ratio decreases 3 to 4 percent, hence free stream Mach number increases approximately 0.4 to 0.5 percent, as the stagnation temperature increases from approximately 625 K to 820 K. Thus, the pitot pressure profiles of figures 10, 13, and 19 and results of figure 22 illustrate the CF_4 tunnel is capable of producing good quality flow at a given value of free stream Mach number and very limited range of free stream Reynolds number. Test section flow conditions for $p_{t,1} \approx 17.6$ MN/m^2 and $T_{t,1} \approx 820$ K are as follows:

$p_\infty = 532.5$ N/m^2	$N_{Re,\infty} = 1.233 \times 10^6/m$
$T_\infty = 271.6$ K	$\rho_2/\rho_\infty = 12.64$
$N_{Pr,\infty} = .761$	$N_{Re,2} = 6.508 \times 10^5/m$
$\gamma_\infty = 1.169$	$p_{t,2} = 21.17$ kN/m^2
$M_\infty = 5.88$	

The values of $N_{Re,\infty}$ and $N_{Re,2}$ in CF_4 are readily attained in the Langley 20-inch Mach 6 air tunnel, thereby providing the capability of examining real-gas (normal-shock density ratio) effects for a given Mach number and Reynolds number.

In figure 23, the average pitot pressure ratio is plotted as a function of axial distance downstream from the nozzle exit z for a nominal stagnation temperature of 717 K and range of stagnation pressure. These data demonstrate the absence of appreciable axial gradients in pitot pressure within the free jet. The average pitot pressure is observed to decrease less than 2 percent between the nozzle exit and 30.5 cm downstream of the exit, corresponding to an increase in Mach number of less than 0.25 percent.

The centerline pitot pressure nondimensionalized by the reservoir stagnation pressure is shown in figure 24 as a function of distance downstream of the nozzle exit for the three values of nominal reservoir temperature. The solid lines in figure 24 denote the mean value of pitot pressure across the inviscid test core. The results of figure 24 illustrate the maximum "peak" value of pitot pressure occurs at the same distance downstream of the nozzle exit for a given reservoir temperature and range of reservoir pressure, and moves upstream with increasing reservoir temperature. For the worst case, the centerline pitot pressure exceeds the average inviscid core pitot pressure by 16 to 18 percent, corresponding to a 1.6 to 2 percent uncertainty in Mach number. In general, the centerline pitot pressure is within 8 percent of the average value across the core, resulting in an uncertainty of 0.8 to 1 percent in Mach number. Thus, a penalty in flow uniformity across the inviscid core must be paid to operate the facility at off-design reservoir conditions, but this penalty may be acceptable for many studies, particularly those involving blunt models.

Shock shape results may be coupled to facility calibration, because these results supply information on the uniformity of the free stream flow (ref. 6). In figure 25, the shock detachment distance measured on a 7.6 cm diameter sphere model is compared to several prediction methods. In general, the measured and predicted values of shock detachment distance are in good agreement and do not indicate any free stream flow nonuniformity (ref. 7). Also, this good agreement lends creditability to the predicted free stream conditions which served as input to the prediction methods.

To examine nozzle flow characteristics on a more sensitive scale, pressure distributions along the center of a sharp-leading-edge flat plate were measured at two reservoir conditions, one being close to nozzle design conditions. The leading edge of the flat plate was positioned 1.27 cm downstream of the nozzle exit and the surface was on the nozzle centerline. The measurements are shown in figure 26, where the surface pressure nondimensionalized by the calculated free stream static pressure is plotted as a function of distance downstream of the leading edge. The flat plate surface pressure initially decreases with distance from the leading edge as expected, then remains essentially constant. These pressure distributions imply the nozzle flow is quite uniform for the present reservoir conditions, being essentially free of disturbances that focus on the nozzle centerline. Also shown in figure 26 are predicted pressure distributions based on weak-interaction theory (ref. 8). The method of reference 8 is observed to overpredict the measured pressure ratio p/p_{∞}, as does the pressure ratio predicted using the measured boundary layer thickness, assuming the displacement thickness is 0.3442 of the boundary layer thickness (ref. 9) and employing oblique shock relations for a

perfect gas. Now, the viscous induced pressure decreases appreciably with decreasing ratio of specific heats. For example, prediction (ref. 8) shows that the pressure ratio at a distance of 16.5 cm from the leading edge is 1.17 for helium (γ_∞ = 5/3), 1.09 for perfect air (γ_∞ = 7/5) and 1.03 for the higher reservoir temperature CF_4 test (γ_∞ = 1.19), with all other inputs held constant for the three test gases. Thus, the flat plate surface pressure is expected to be close to free stream static, although not quite as close as shown in figure 26, especially for the higher $T_{t,1}$ test. It should be noted that the free stream static pressure based on vibrationally relaxing flow will be less than that for equilibrium flow; hence, a small departure from equilibrium would result in an increase in p/p_∞. A second possible contributor is the experimental uncertainty for the input pitot pressure is approximately 2 percent, corresponding to a 4-percent uncertainty in calculated free stream pressure. In any case, these flat plate data demonstrate the existence of disturbance-free flow at the test section for the two reservoir conditions examined, and provide creditability to predicted free stream conditions.

As discussed previously, a slight sandblasting of the model occurs during a test. As experienced in hotshot wind tunnels, flow contaminants can result in a substantial increase in heating rate beyond that for clean flow (ref.10). For this reason, heat transfer distributions were measured on a 10.16 cm diameter hemisphere cylinder using the thin-skin calorimeter technique with chromel-alumel thermocouples. The reservoir pressure was 6.9 MN/m^2 and the reservoir temperature was 706 K, corresponding to a free stream Mach number of 6.04. These data are compared to prediction in figure 27, where the heat transfer rate is plotted as a function of the angle subtended by a circular arc measured from the sphere axis of symmetry through the stagnation point θ. The predicted heating distribution for this CF_4 test was furnished by the author of reference 11. The measured stagnation point heating rate is approximately 8 percent less than predicted, and reasonably good agreement exists between the measured and predicted heat transfer distribution. Thus, the present level of flow contaminants does not have an appreciable influence on measured heat transfer rates using the thin skin technique.

CONCLUDING REMARKS

A detailed description of the Langley hypersonic CF_4 tunnel is presented along with discussion of the basic components, instrumentation, and operating procedure. Operational experience with the CF_4 reclaimer and lead-bath heater is discussed.

Pitot pressure surveys were measured at the nozzle exit and downstream of the exit for nominal reservoir temperatures of 608 K, 717 K, and 815 K and range of reservoir pressure from 6.9 to 17.6 MN/m^2. At the maximum value of reservoir pressure and temperature, which corresponds to the reservoir conditions for which the contoured axisymmetric nozzle was designed, a uniform

test core having a diameter of approximately 28 cm (0.55 times the nozzle exit diameter) exists. The corresponding free stream Mach number is 5.9, unit Reynolds number is 1.2×10^6 per meter, ratio of specific heats is 1.17 and the normal shock density ratio is equal to 12.6. When the facility is operated at reservoir pressures and temperatures below the design values, "dips" and "spikes" occur on the centerline pitot pressure, indicating the existence of flow disturbances originating in the upstream region of the nozzle. These "dips" and "spikes" are relatively small in magnitude, and, in general, result in a perturbation in centerline free stream Mach number of less than 1 percent. A slight decrease in average pitot pressure across the test core with distance downstream of the nozzle was observed, with the corresponding free stream Mach number variation being about 0.3 percent for a distance of 20.3 cm. Comparison of measured and predicted shock detachment distance on a sphere and pressure distributions measured on a sharp leading-edge flat plate revealed the absence of significant flow nonuniformity and lent creditability to predicted free stream flow conditions.

The economic operation of this facility centers about the CF_4 reclaimer, which was designed to operate at an efficiency of 90 to 95 percent. A number of modifications have been made to the reclaimer system to improve its performance, and presently the system reclaims approximately 75 percent of the test gas. Even with current budgetary constraints, this efficiency permits the CF_4 tunnel to be operated as a viable research wind tunnel.

REFERENCES

1. Jones, Robert A.; and Hunt, James L.: Use of Tetrafluoromethane to Simulate Real-Gas Effects on the Hypersonic Aerodynamics of Blunt Vehicles. NASA TR R-312, 1969.

2. Schaefer, William T., Jr.: Characteristics of Major Active Wind Tunnels at the Langley Research Center. NASA TM X-1130, 1965.

3. Johnson, Charles B.; Boney, Lillian R.; Ellison, James C.; and Erickson, Wayne D.: Real-Gas Effects on Hypersonic Nozzle Contours With a Method of Calculation. NASA TN D-1622, 1963.

4. Burner, Alpheus W.; and Midden, Raymond E.: Holographic Flow Visualization at the Langley CF_4 Tunnel. NASA TM 74051, 1977.

5. Hunt, James L.; and Boney, Lillian R.: Thermodynamic and Transport Properties of Gaseous Tetrafluoromethane in Chemical Equilibrium. NASA TN D-7181, 1973.

6. Miller, Charles G., III: Shock Shapes on Blunt Bodies in Hypersonic-Hypervelocity Helium, Air, and CO_2 Flows, and Calibration Results in Langley 6-Inch Expansion Tube. NASA TN D-7800, 1975.

7. Miller, Charles G., III: A Comparison of Measured and Predicted Sphere Shock Shapes in Hypersonic Flows With Density Ratios From 4 to 19. NASA TN D-8076, 1975.

8. Bertram, Mitchel H.; and Blackstock, Thomas A.: Some Simple Solutions to the Problem of Predicting Boundary-Layer Self-Induced Pressures. NASA TN D-798, 1961.

9. Schlichting, Hermann: Boundary Layer Theory. Sixth Edition, McGraw-Hill, Inc., p. 130, 1968.

10. Grabau, Martin; Smithson, H. K., Jr.; and Little, Wanda J.: A Data Reduction Program for Hotshot Tunnels Based on the Fay-Riddell Heat-Transfer Rate Using Nitrogen at Stagnation Temperatures From 1500 to 5000° K. AEDC-TDR-64-50, 1964.

11. Sutton, Kenneth; and Graves, Randolph A., Jr.: A General Stagnation-Point Convective-Heating Equation for Arbitrary Gas Mixtures. NASA TR R-376, 1971.

TABLE I. - MEASURED AND PREDICTED FLOW CONDITIONS

	Measured Quantities				Predicted Quantities					
Test	z, cm	$P_{t,1}$, MN/m^2	$T_{t,1}$, K	$P_{t,2}$, kN/m^2	p_∞, N/m^2	T_∞, K	M_∞	$N_{Re,\infty}$, m^{-1}	$\frac{\rho 2}{\rho_\infty}$	$N_{Re,2}$, m^{-1}
207	0	7.25	618	8.98	185	156	6.30	$.927\times10^6$	11.74	3.89×10^5
208	0	12.16	627	15.20	315	159	6.29	1.497	11.80	6.50
209	0	17.66	632	22.08	456	160	6.31	2.132	11.85	9.44
206	10.16	7.22	617	9.03	186	155	6.29	.937	11.72	3.93
205	10.16	12.33	626	15.38	317	158	6.29	1.531	11.79	6.60
204	10.16	17.38	623	21.48	435	154	6.36	2.197	11.80	9.30
201	20.32	6.76	584	8.51	165	136	6.43	1.061	11.51	4.14
202	20.32	11.89	607	14.87	295	147	6.38	1.647	11.67	6.54
203	20.32	17.71	619	22.04	443	152	6.37	2.310	11.78	9.61
186	0	6.81	681	8.37	187	192	6.11	.718	12.06	3.22
187	0	12.01	708	14.73	336	206	6.07	1.160	12.20	5.53
182	0	17.95	722	21.97	506	212	6.07	1.665	12.29	7.85
185	2.54	7.21	725	8.71	204	218	6.01	.642	12.26	3.08
184	2.54	12.05	733	14.68	344	221	6.01	1.057	12.30	5.04
183	2.54	17.98	735	21.89	510	220	6.04	1.584	12.34	7.68
190	5.08	7.12	708	8.72	201	208	6.04	.680	12.18	3.16
189	5.08	12.26	708	15.97	341	206	6.08	1.178	12.20	5.59
188	5.08	17.68	708	21.35	483	203	6.12	1.705	12.24	7.78
193	10.16	7.14	704	8.64	198	205	6.06	.686	12.17	3.16
192	10.16	12.26	713	14.94	342	208	6.06	1.158	12.22	5.49
191	10.16	17.64	716	21.62	495	208	6.09	1.678	12.26	7.80
196	20.32	7.10	702	8.64	198	204	6.06	.690	12.16	3.17
195	20.32	12.35	712	15.08	345	208	6.07	1.173	12.22	5.56
194	20.32	16.78	712	20.42	466	206	6.09	1.609	12.24	7.41
200	30.48	7.41	698	8.97	204	202	6.08	.727	12.15	3.29
198	30.48	12.48	702	15.14	342	202	6.10	1.220	12.18	5.77
197	30.48	17.73	702	21.48	482	199	6.13	1.757	12.21	7.91
213	0	7.88	811	9.49	240	268	5.85	.556	12.54	2.96
212	0	12.62	821	15.19	384	272	5.86	.881	12.60	4.62
211	0	17.64	823	21.17	532	272	5.88	1.233	12.64	6.51
214	10.16	7.07	809	8.48	215	267	5.85	.499	12.54	2.67
215	10.16	12.10	829	14.51	368	277	5.85	.838	12.63	4.37
216	10.16	17.84	841	21.46	546	282	5.86	1.247	12.70	6.38
219	20.32	7.16	789	8.43	209	255	5.90	.514	12.49	2.73
218	20.32	12.32	801	14.60	362	260	5.90	.871	12.55	4.48
217	20.32	17.48	803	20.82	515	259	5.92	1.244	12.58	6.62

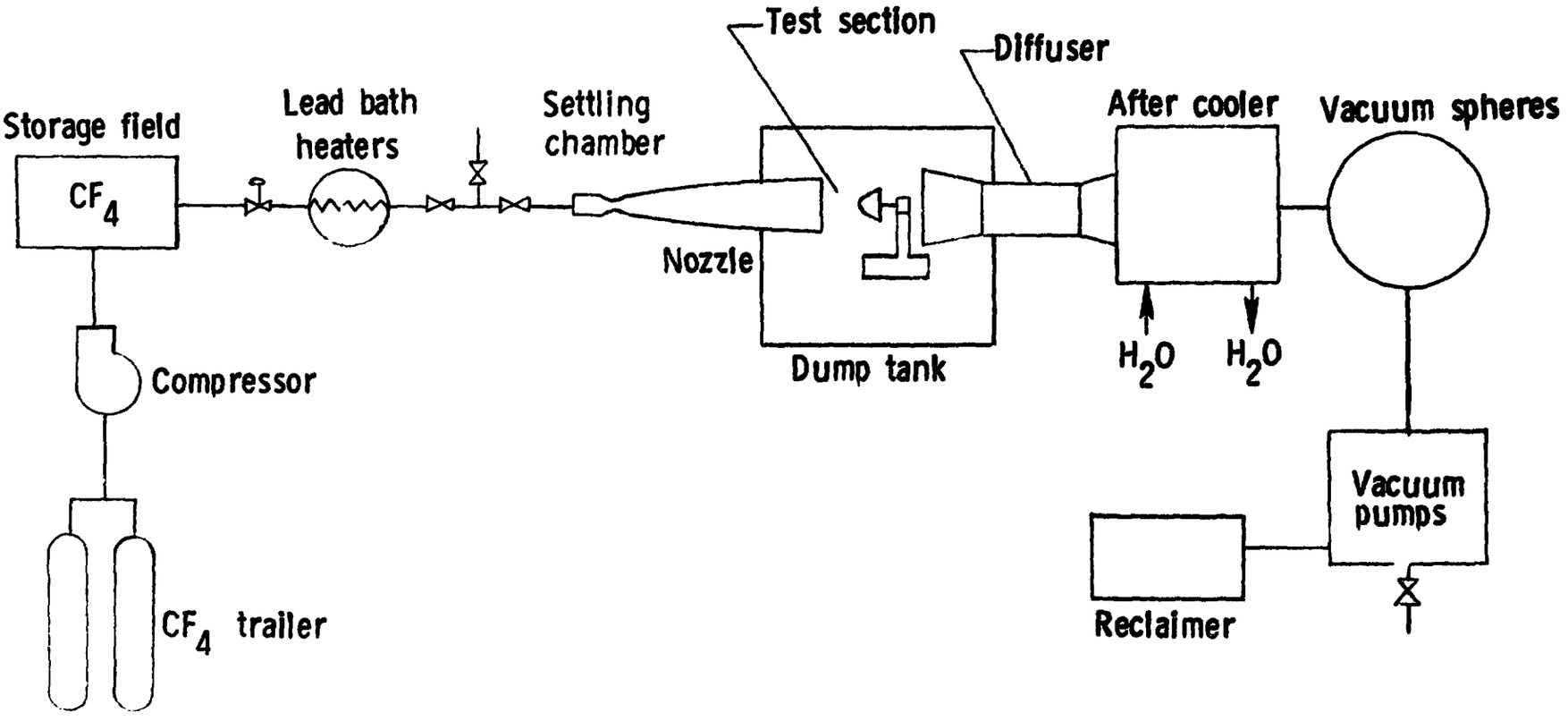

(a) Schematic.

Figure 1. - Schematic drawing and photograph of Langley hypersonic CF_4 tunnel.

(b) Photograph.

Figure . - Concluded.

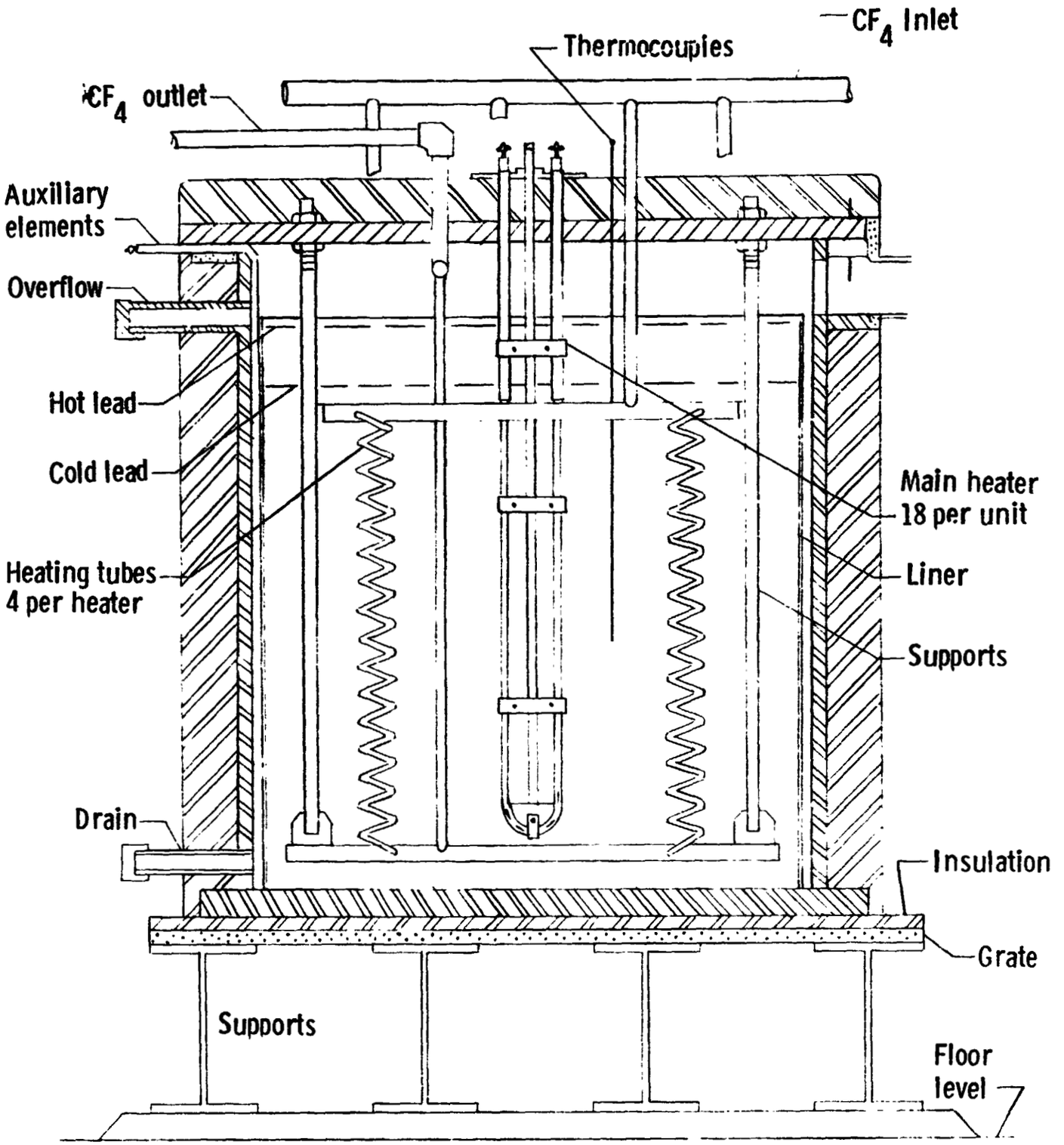

Figure 2. - Sketch of lead-bath heater.

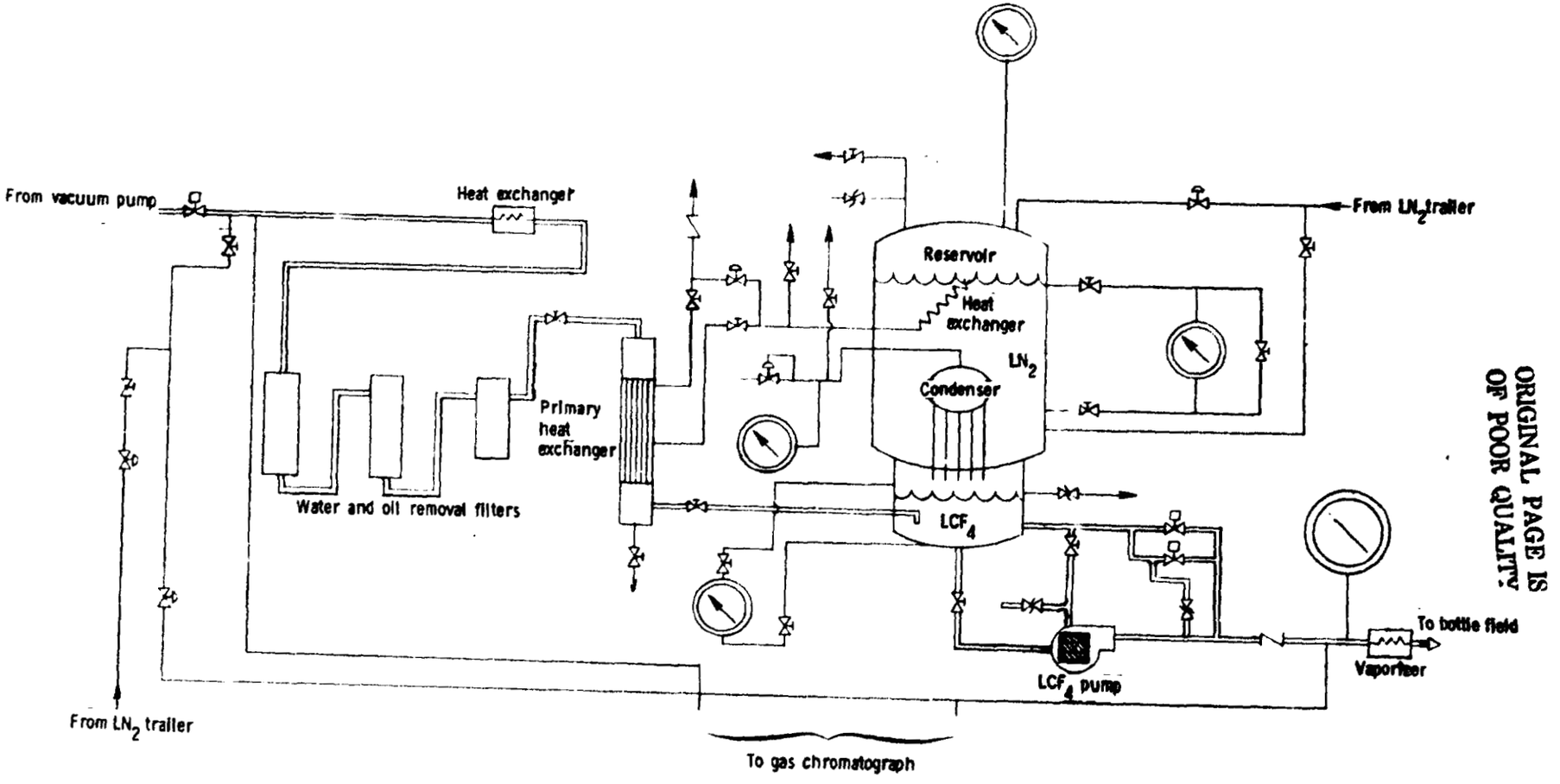

Figure 3. - Schematic drawing of CF_4 reclaimer system.

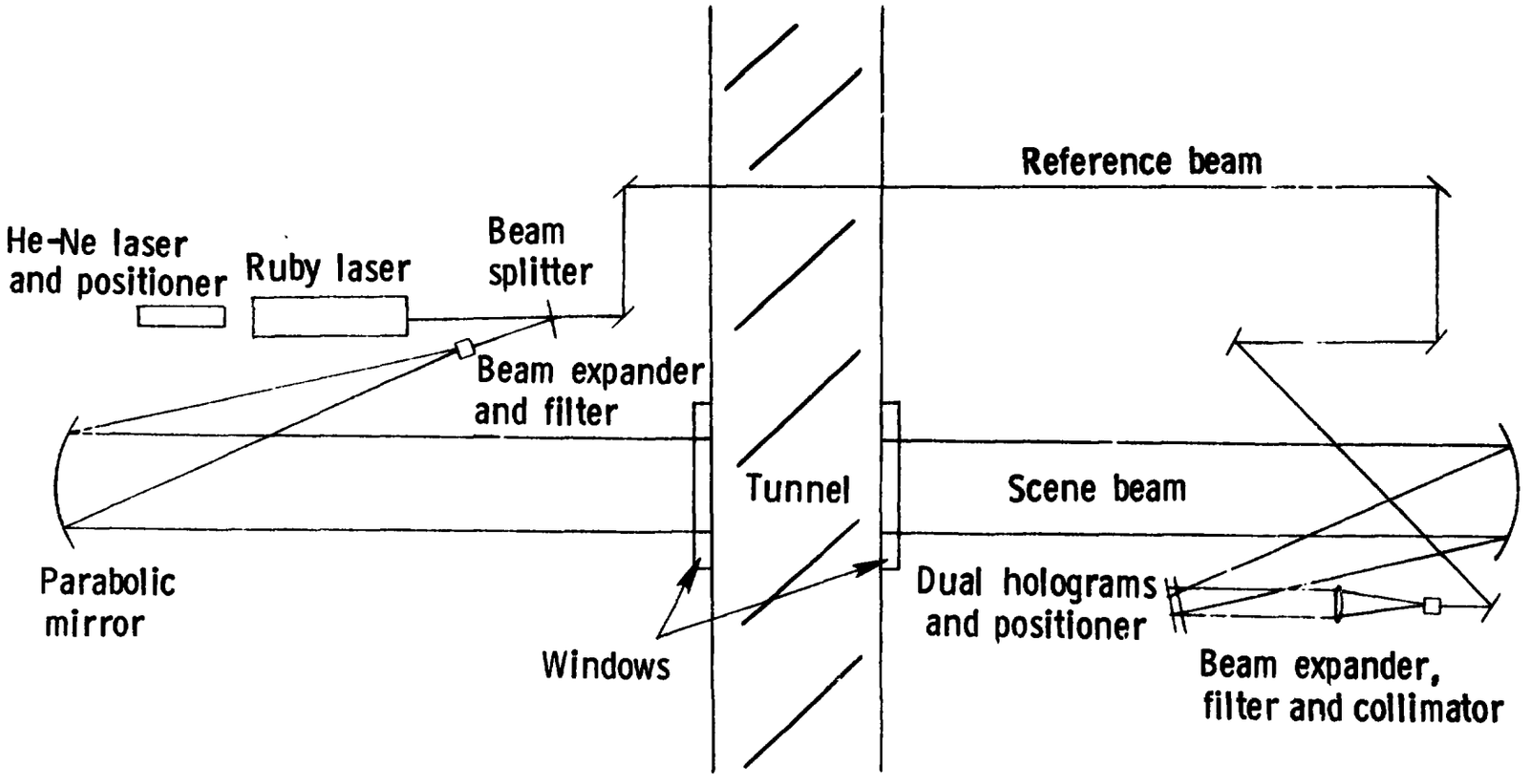

Figure 4. - Holographic system for CF_4 tunnel.

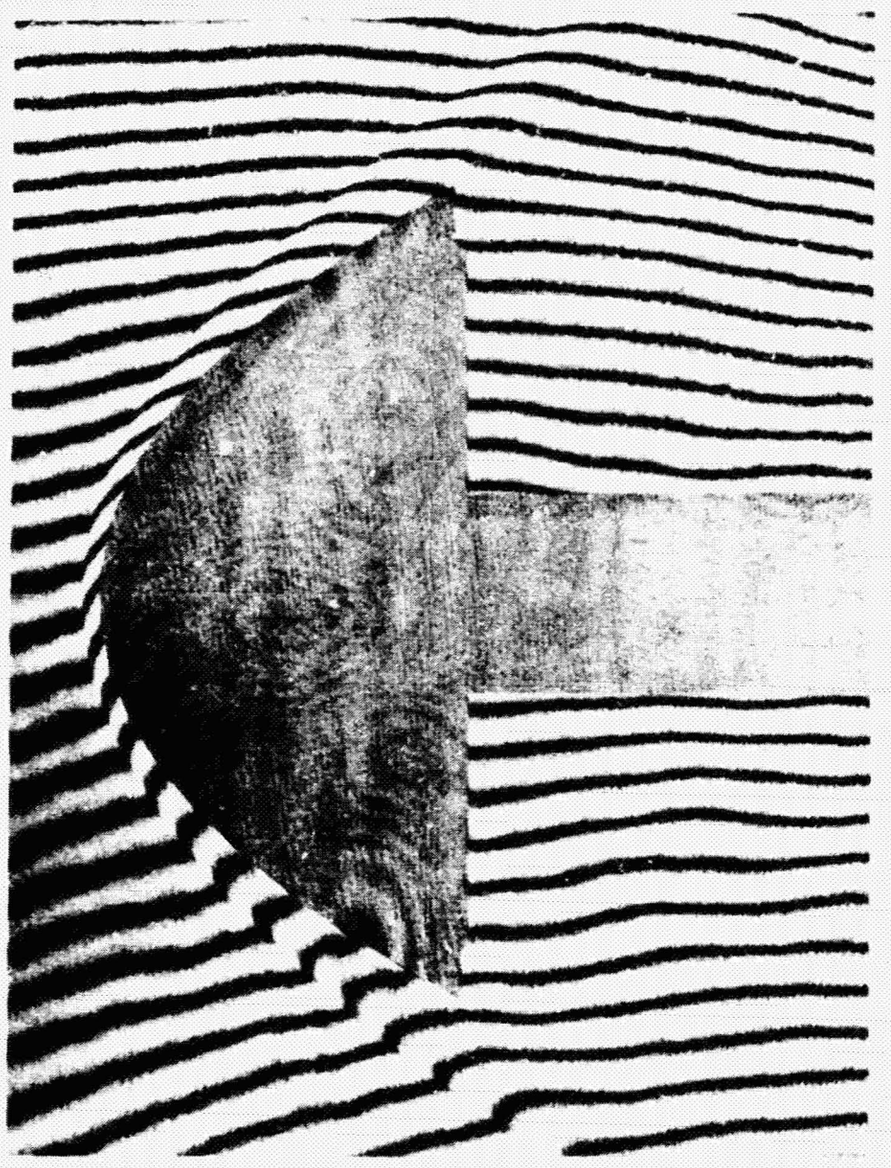

Figure 5. - Representative interferogram for parabolic model at zero angle of attack.

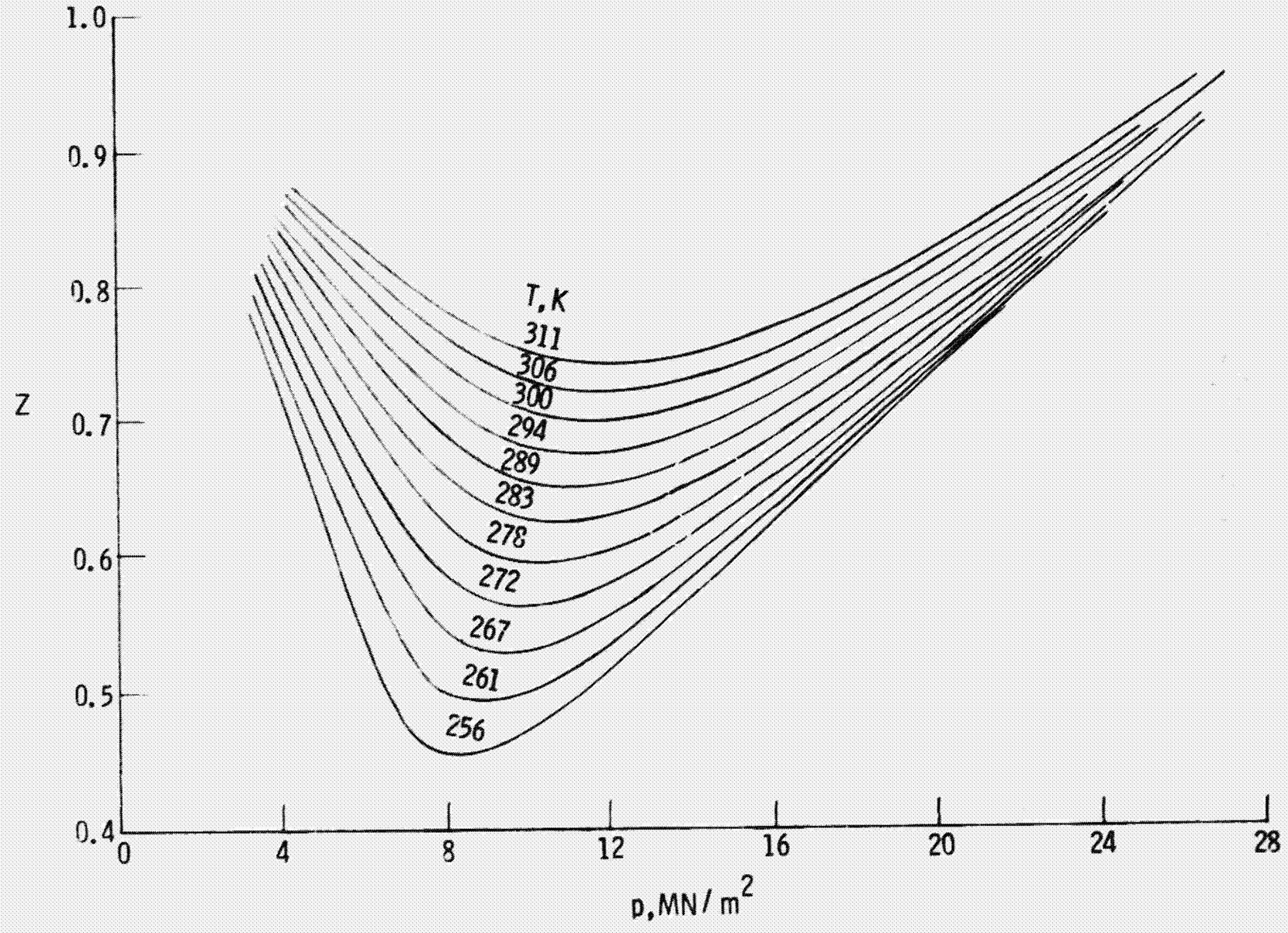

Figure 6. - Compressibility factor for CF_4 as a function of pressure for various values of temperature.

Figure 7. - Photograph of stainless steel screen removed from the settling chamber following decrease in facility performance.

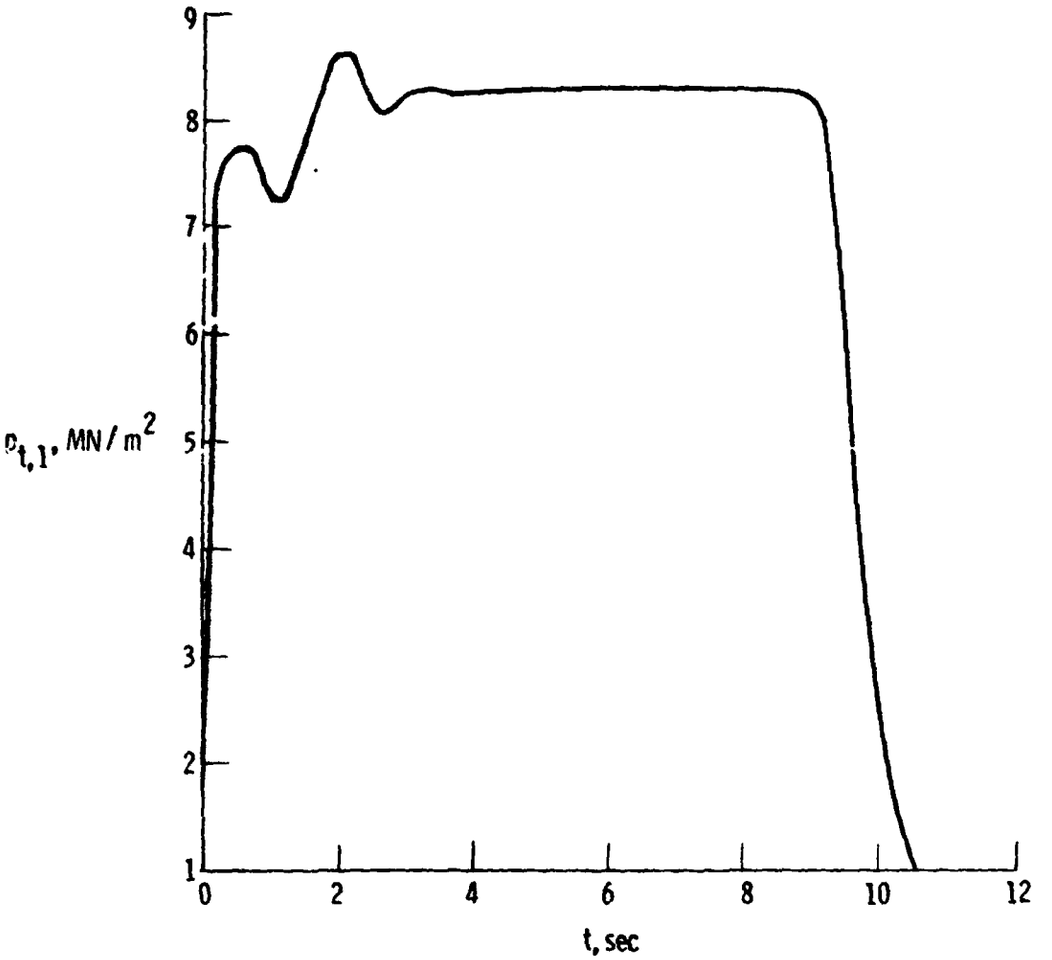

(a) Reservoir stagnation pressure.

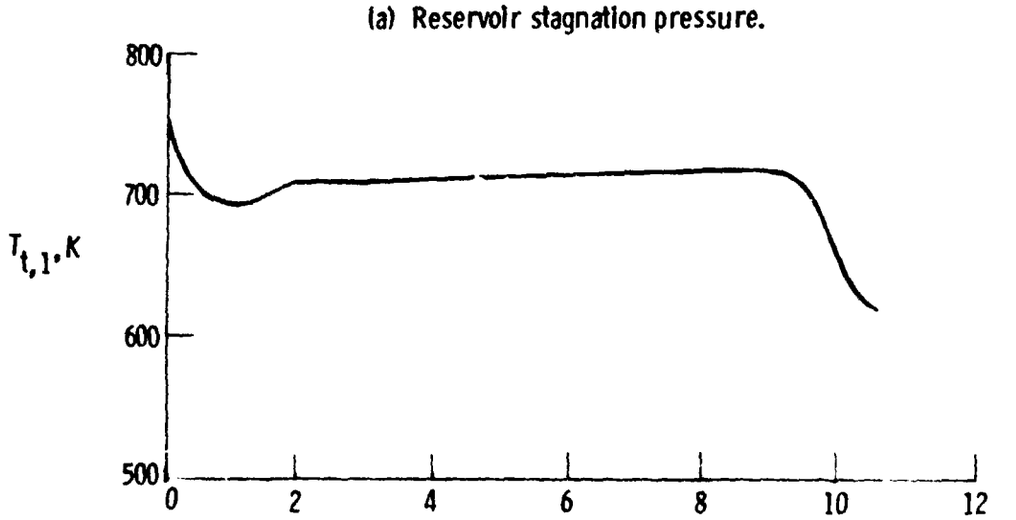

(b) Reservoir stagnation temperature.

Figure 8. - Reservoir stagnation pressure, reservoir stagnation temperature, and pitot pressure as a function of time.

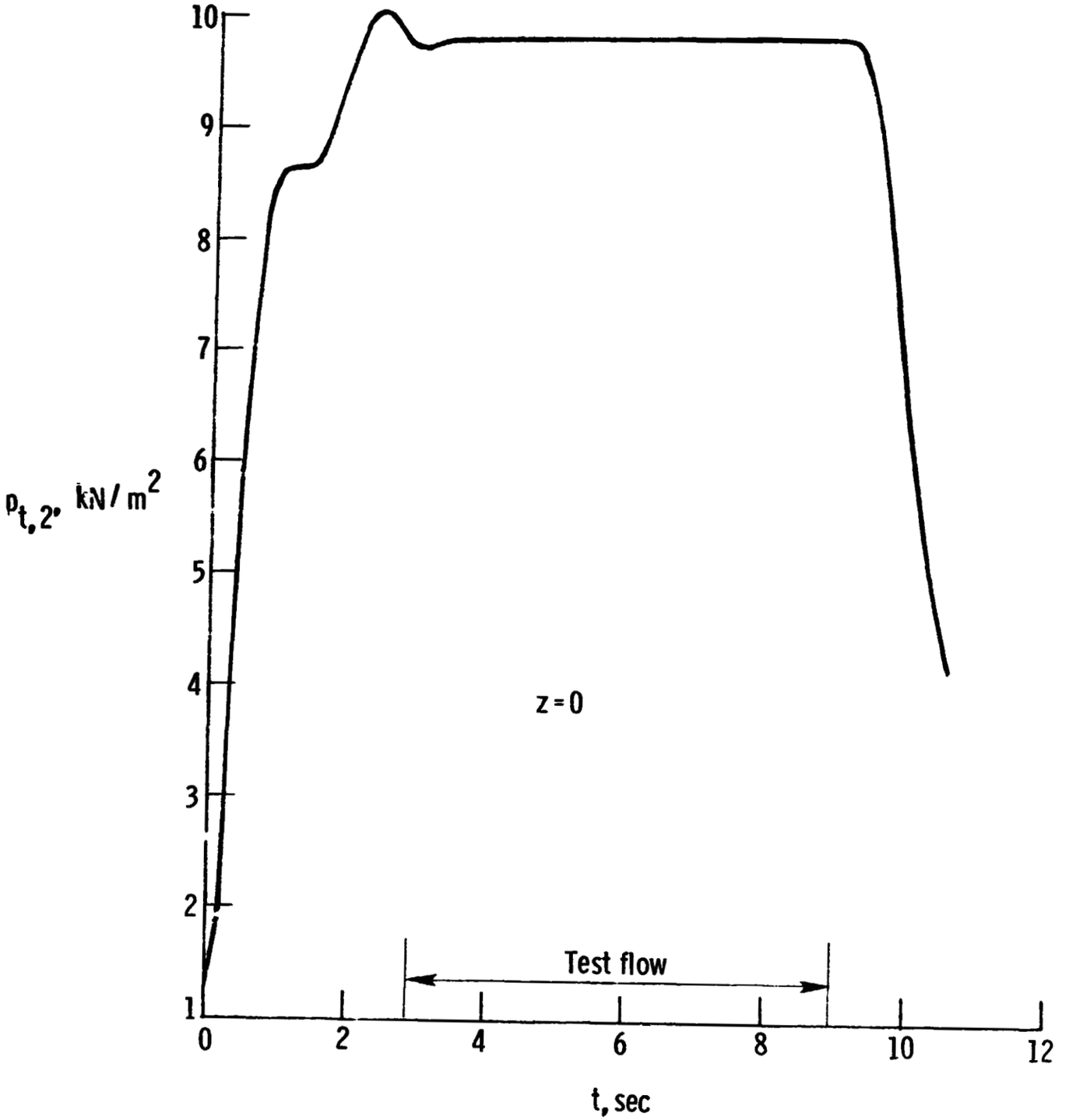

(c) Pitot pressure.

Figure 8. - Concluded.

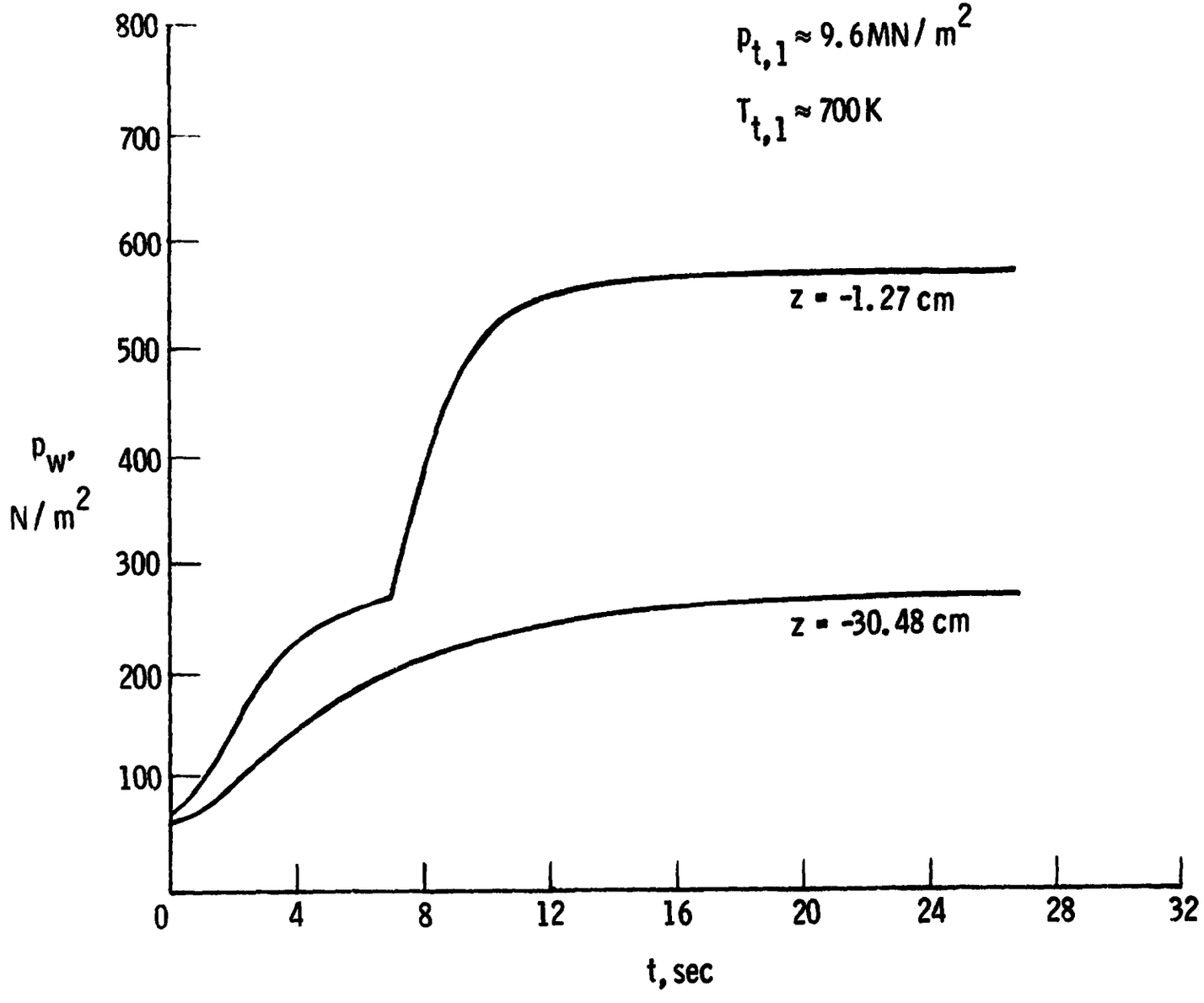

Figure 9. - Nozzle wall pressure as a function of run time.

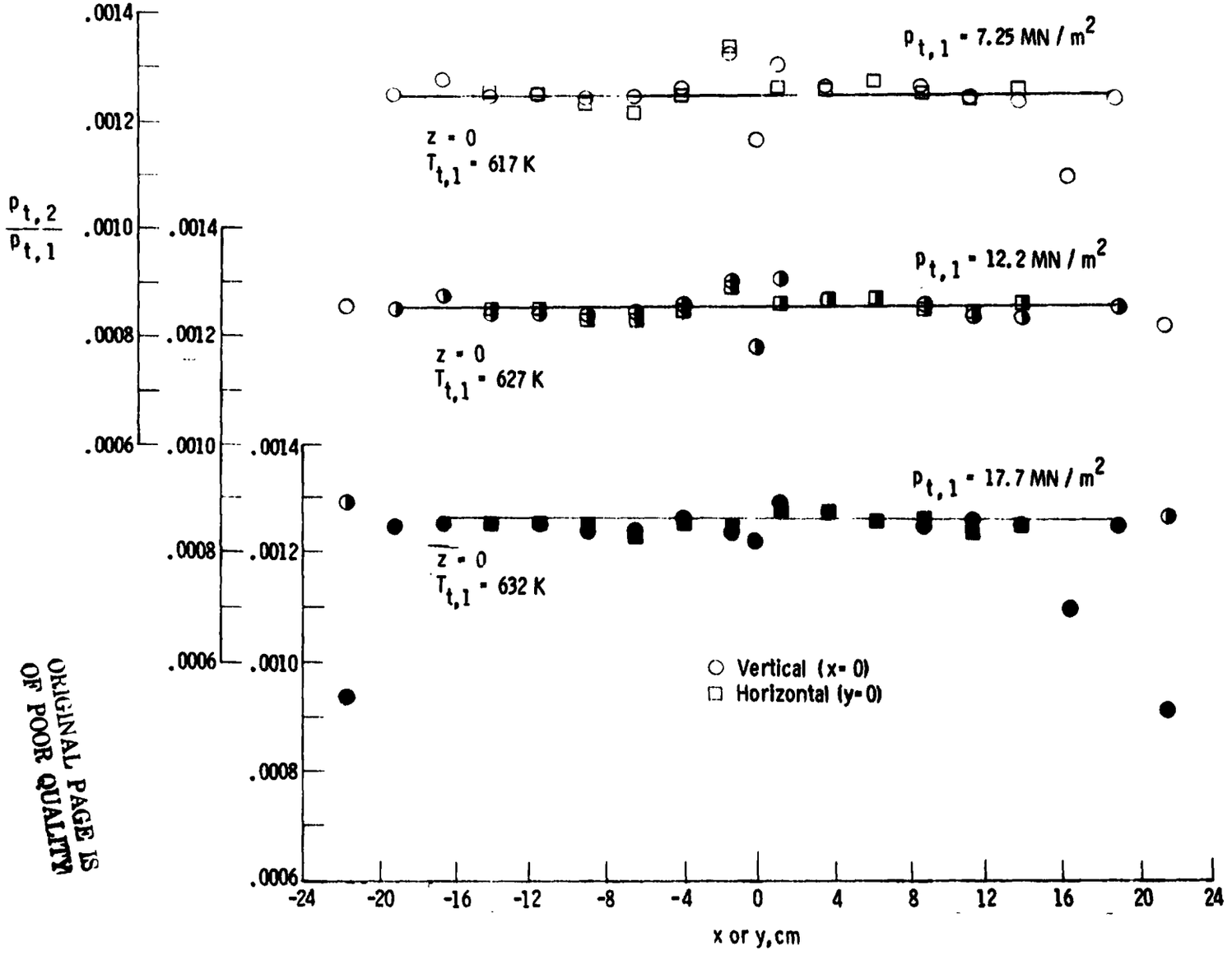

Figure 10. - Pitot pressure at nozzle exit for $\overline{T}_{t,1} \approx 608$ K and various values of $p_{t,1}$.

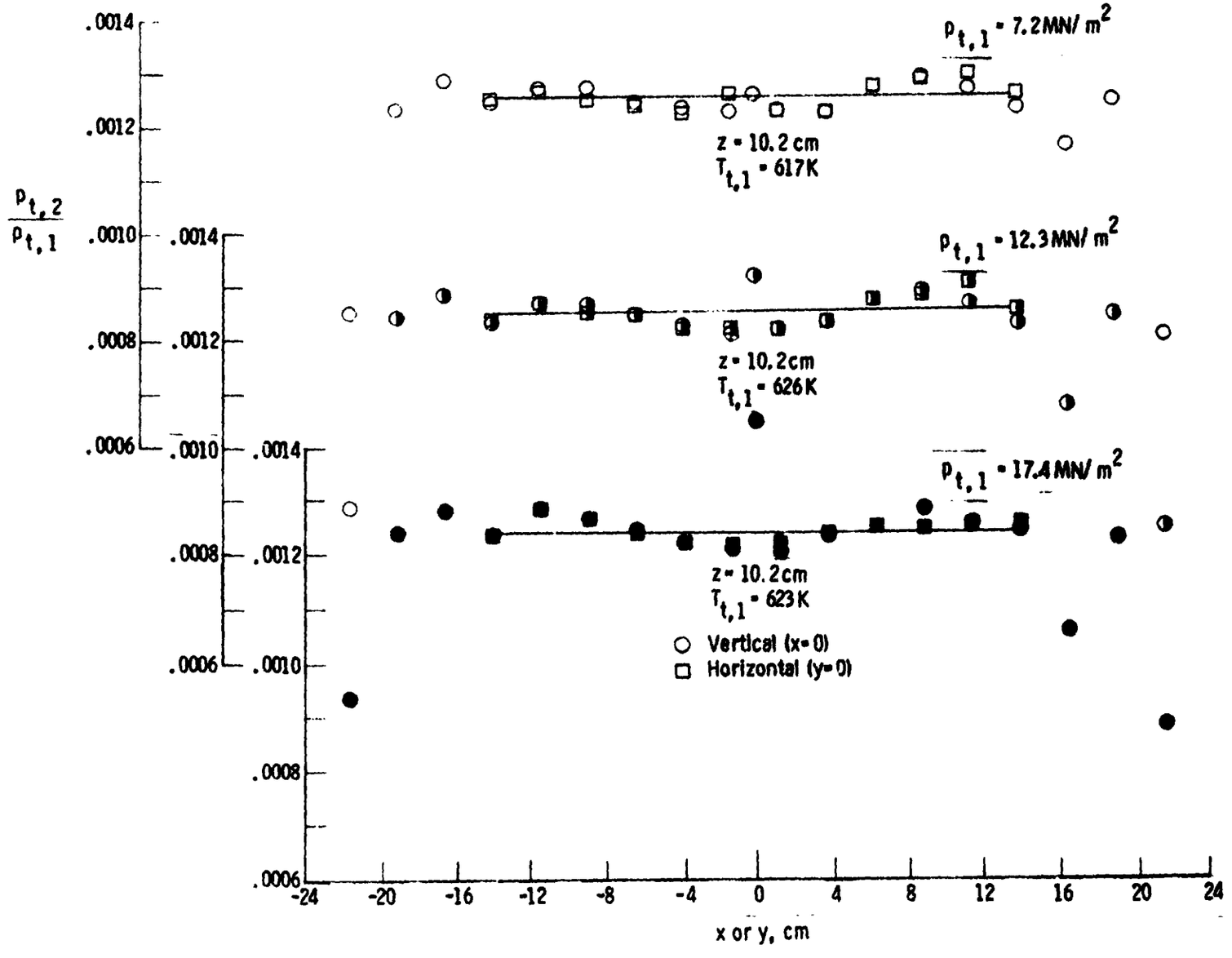

Figure 11. - Pitot pressure profiles 10.2cm downstream of nozzle exit for $\bar{T}_{t,1} \approx 608$ K and various values of $p_{t,1}$.

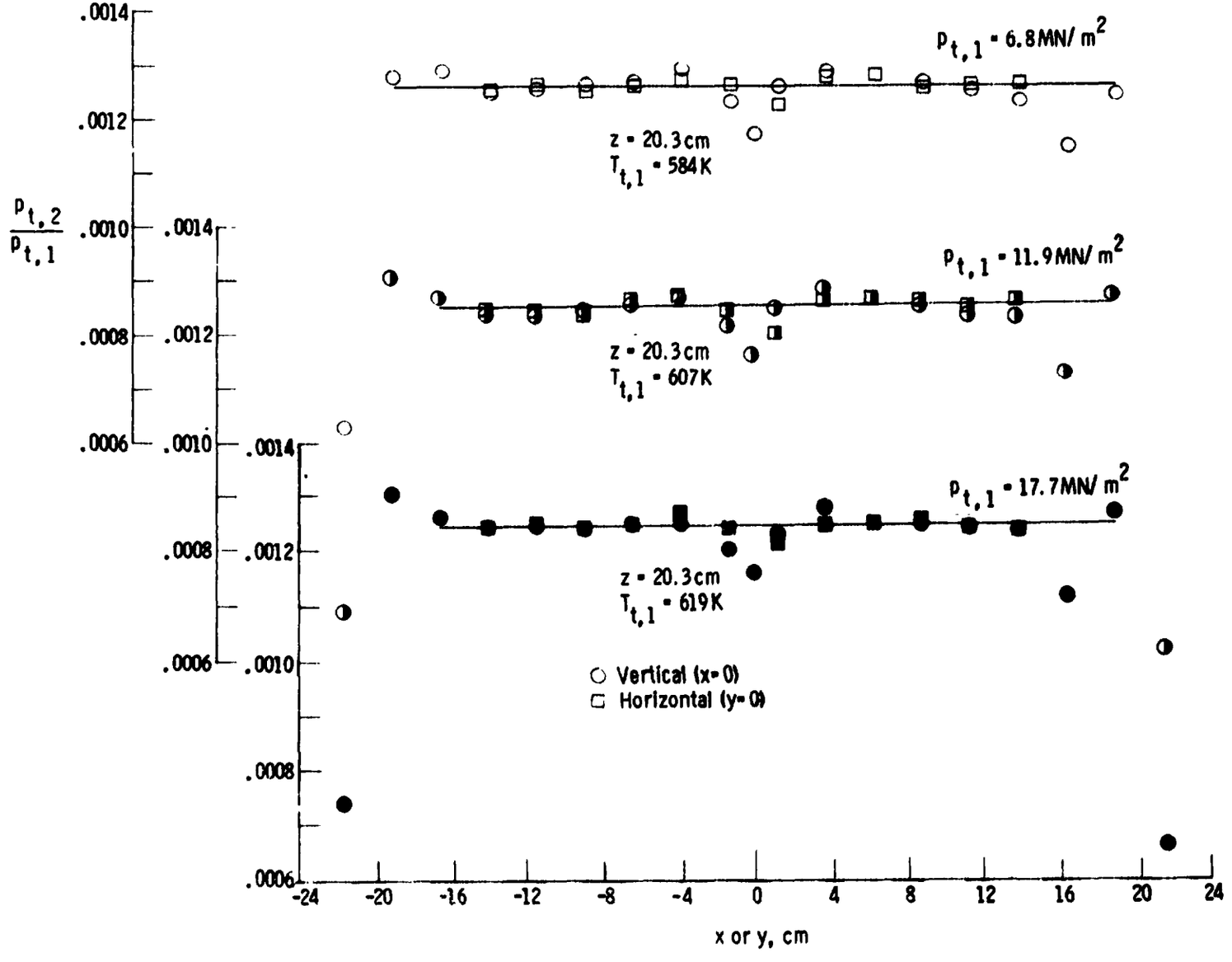

Figure 12. - Pitot pressure profiles 20.3 cm downstream of nozzle exit for $\overline{T}_{t,1} \approx 608$ K and various values of $p_{t,1}$.

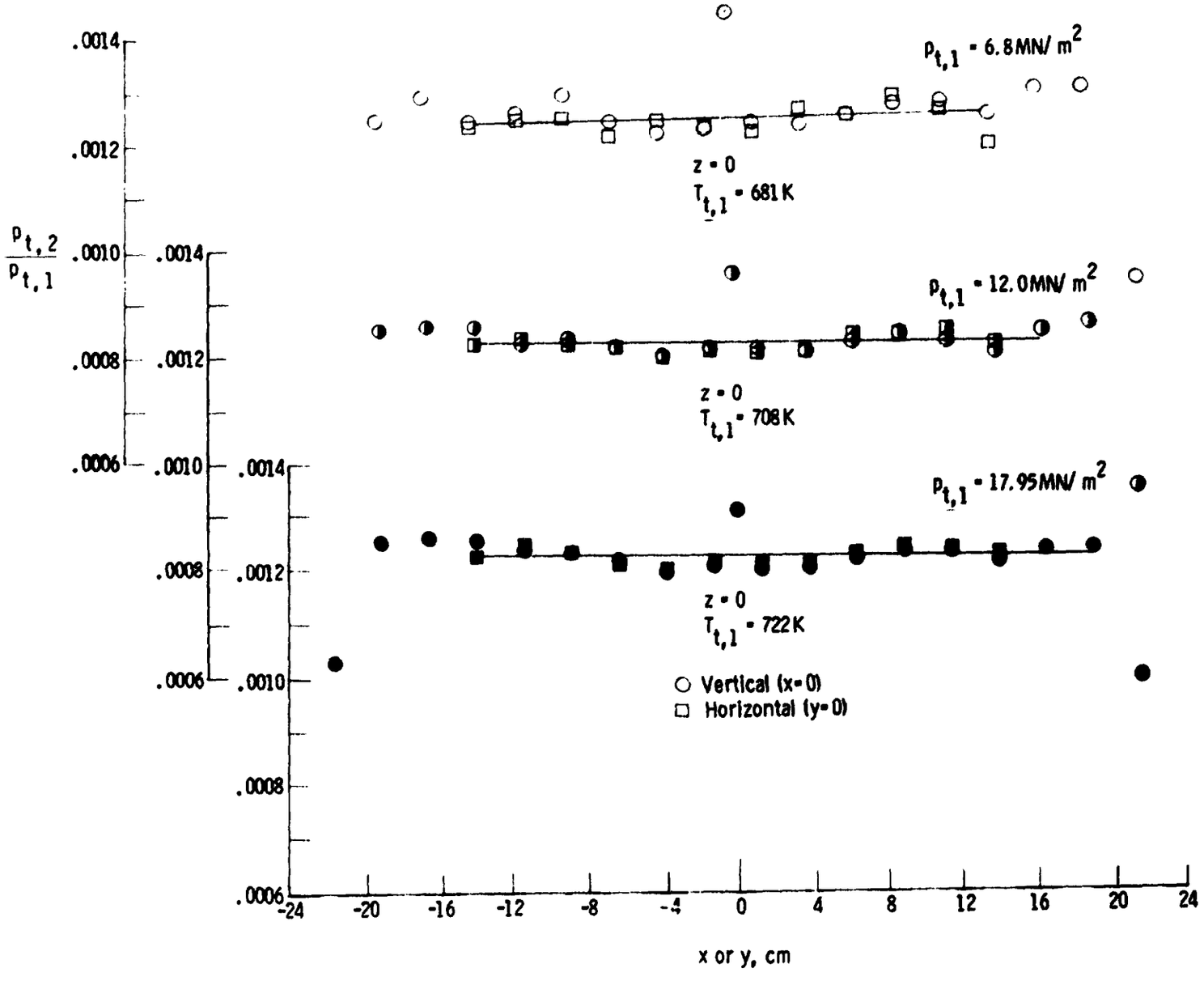

Figure 13. - Pitot pressure profiles at nozzle exit for $\bar{T}_{t,1} \approx 717$ K and various values of $p_{t,1}$.

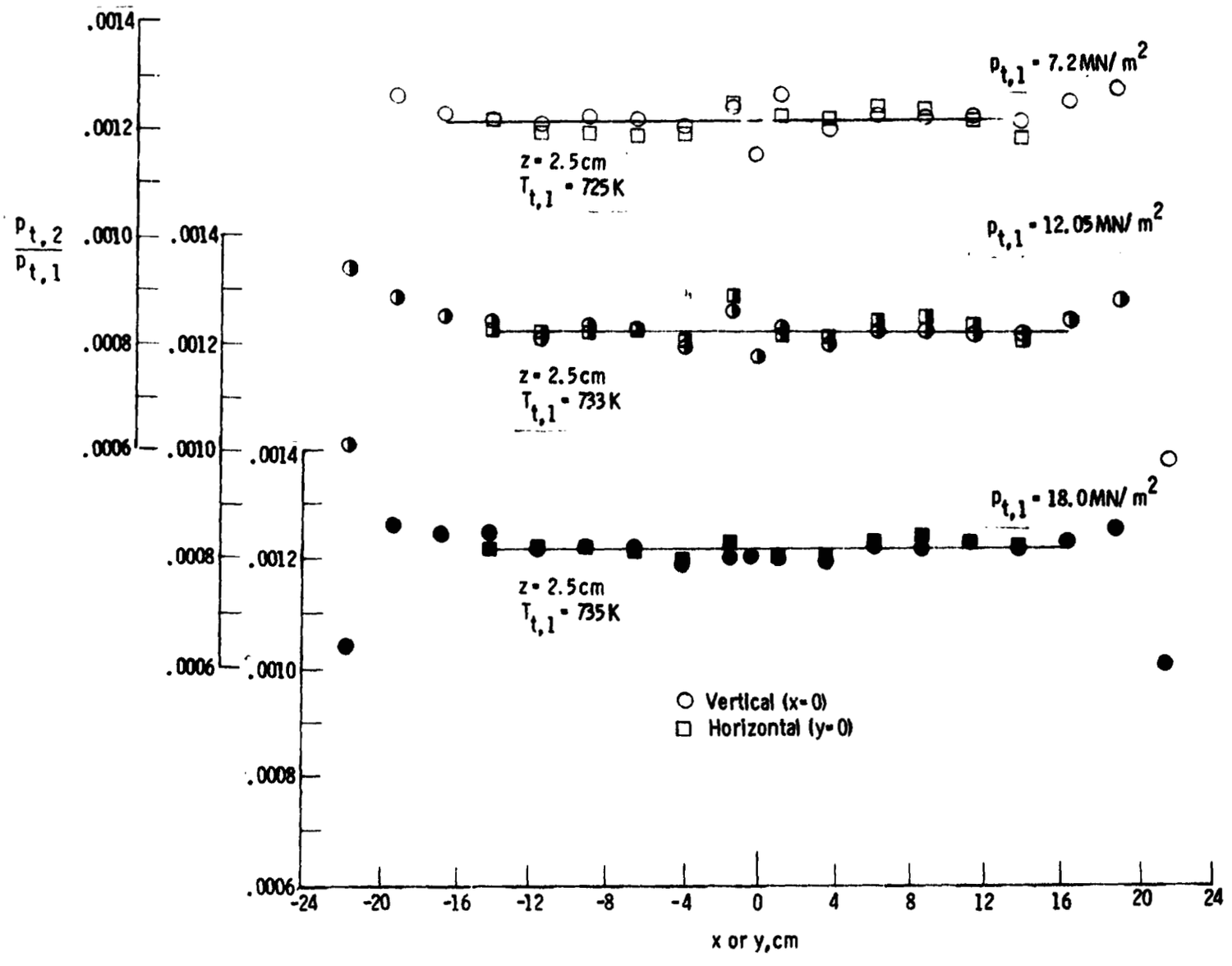

Figure 14. - Pitot pressure profiles 2.5cm downstream of nozzle exit for $\overline{T}_{t,1} \approx 717$ K and various values of $p_{t,1}$.

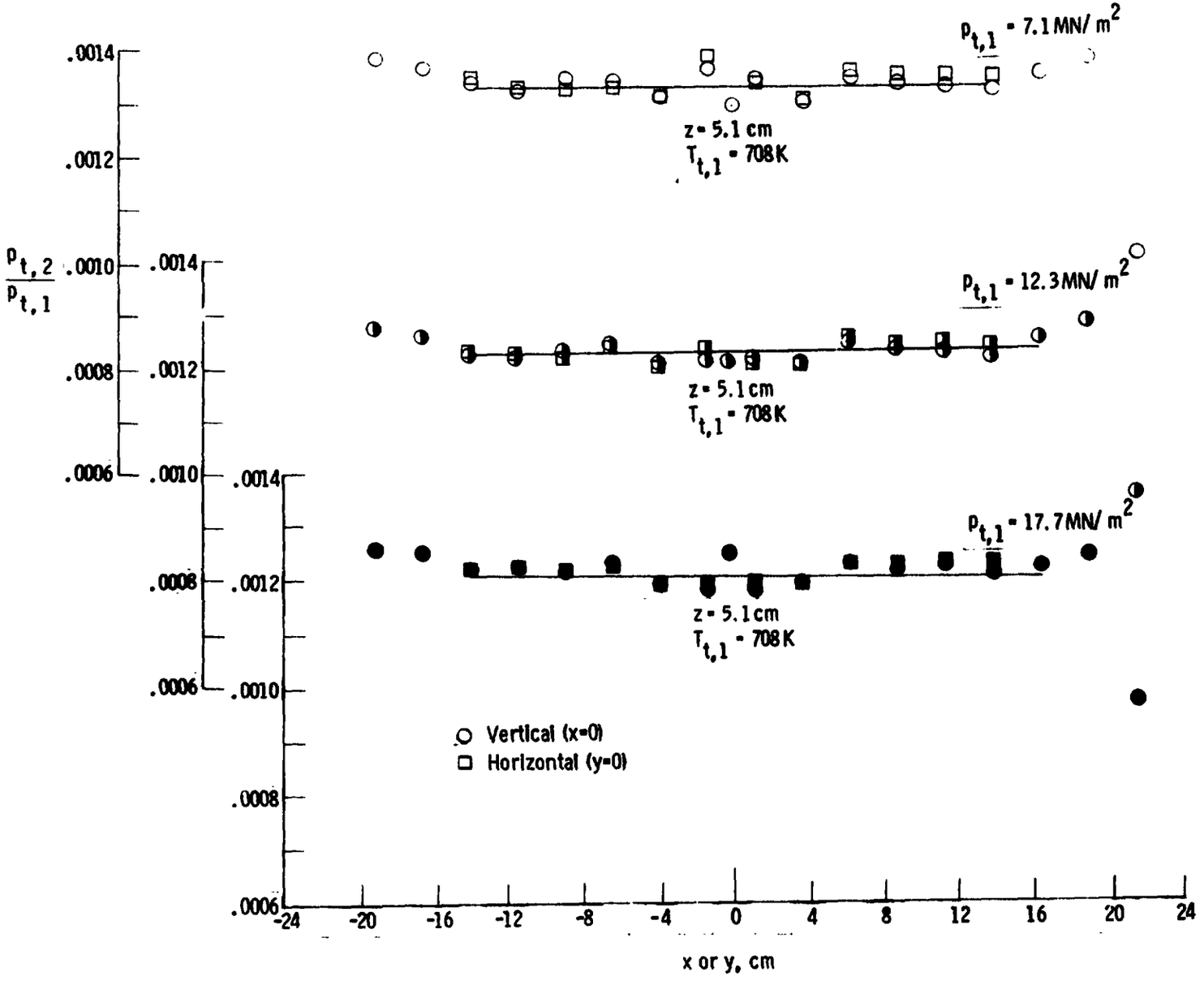

Figure 15. - Pitot pressure profiles 5.1 cm downstream of nozzle exit for $\overline{T}_{t,1} \approx 717$K and various values of $p_{t,1}$.

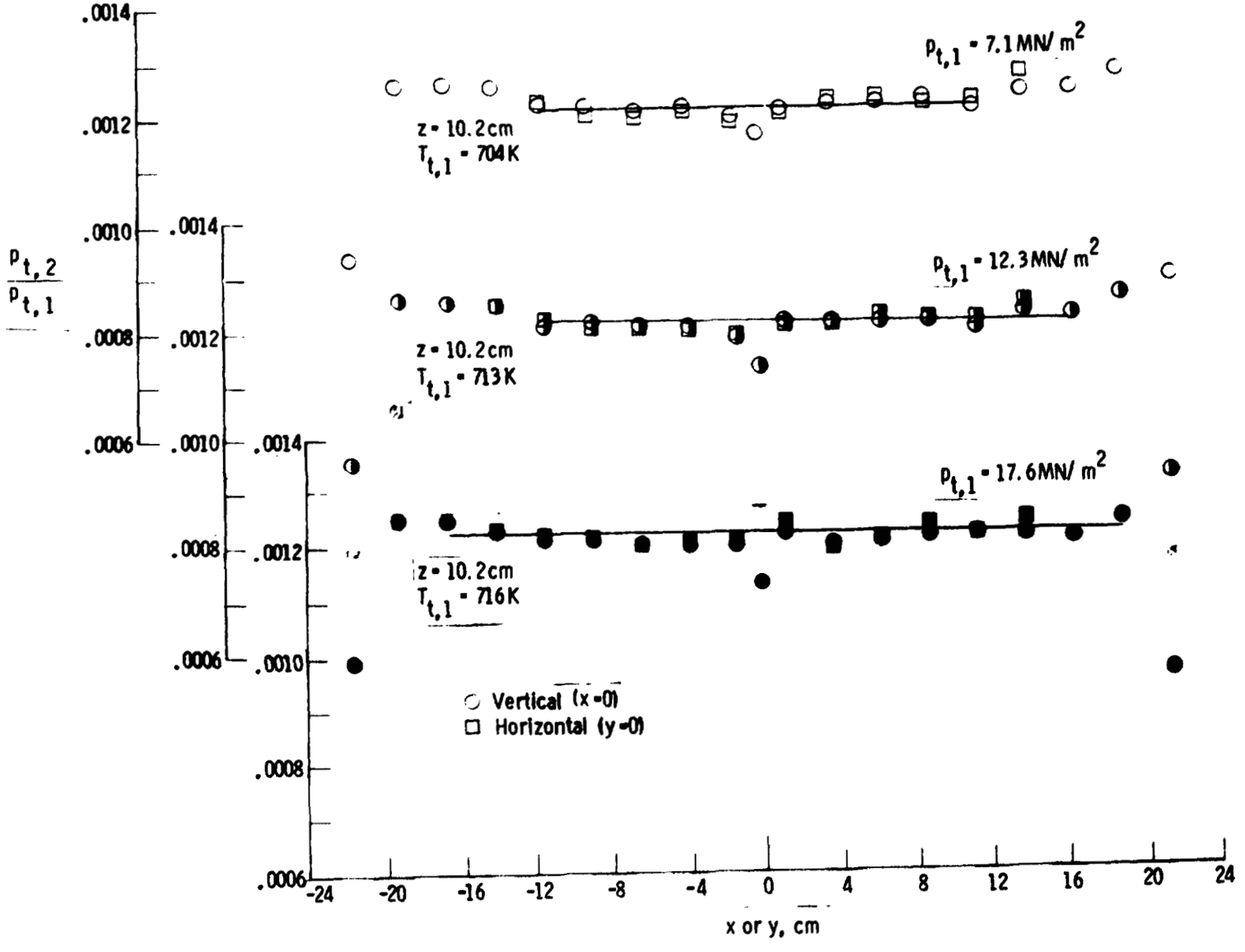

Figure 16. - Pitot pressure profiles 10.2 cm downstream of nozzle exit for $\overline{T}_{t,1} \approx 717$ K and various values of $p_{t,1}$.

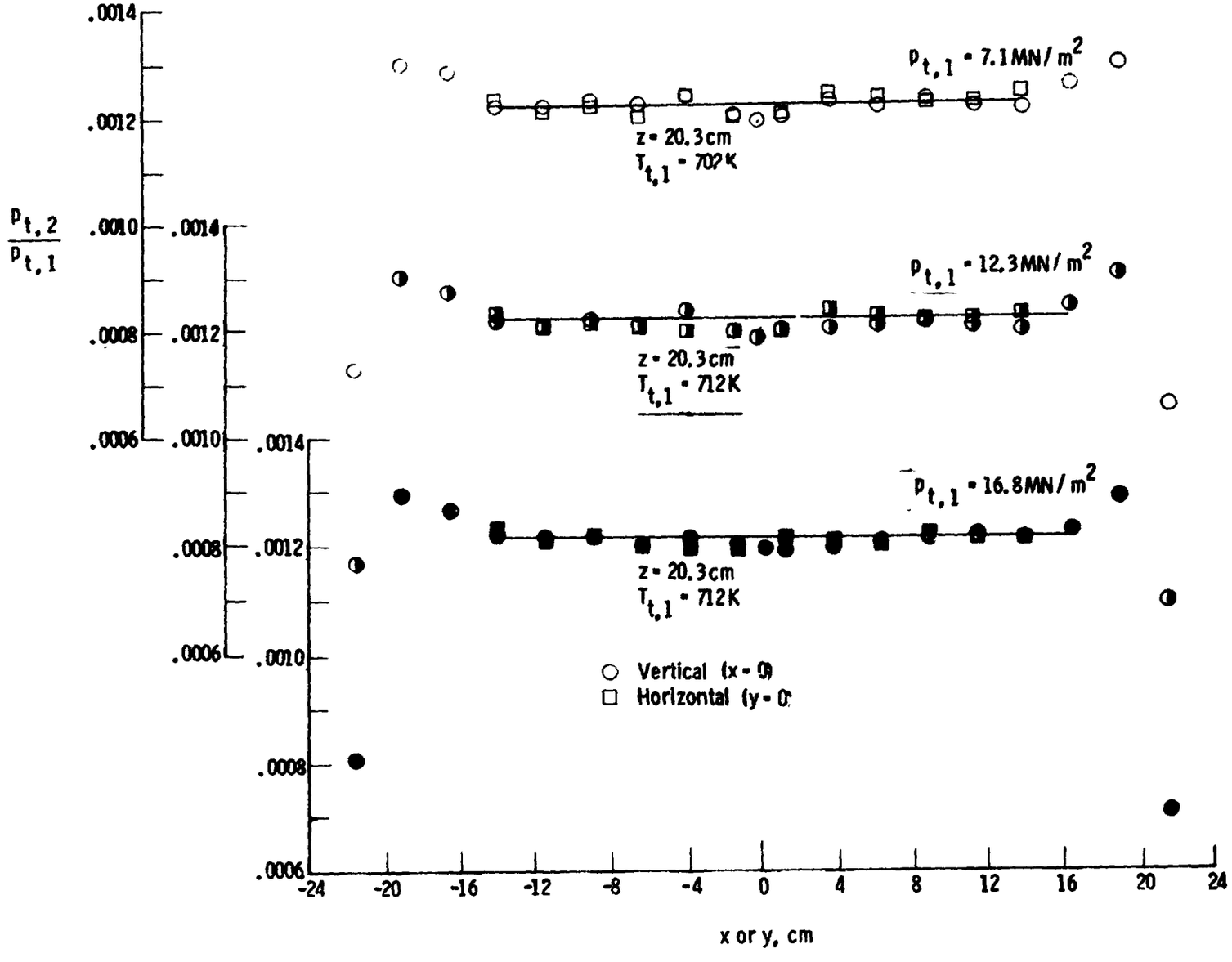

Figure 17. - Pitot pressure profiles 20.3 cm downstream of nozzle exit for $\bar{T}_{t,1} \approx 717$K and various values of $p_{t,1}$.

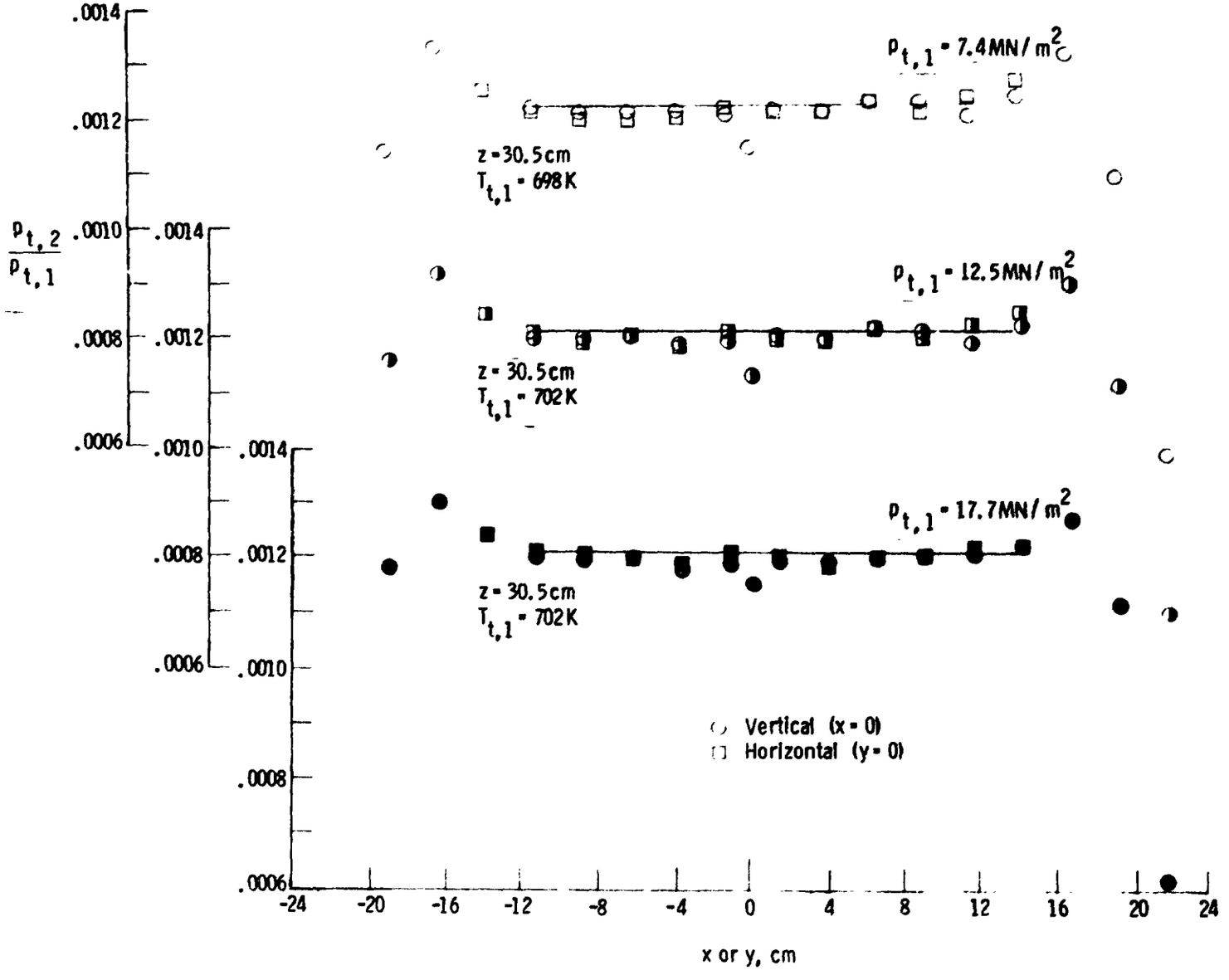

Figure 18. - Pitot pressure profiles 30.5cm downstream of nozzle exit for $\bar{T}_{t,1} \approx 717$K and various values of $p_{t,1}$.

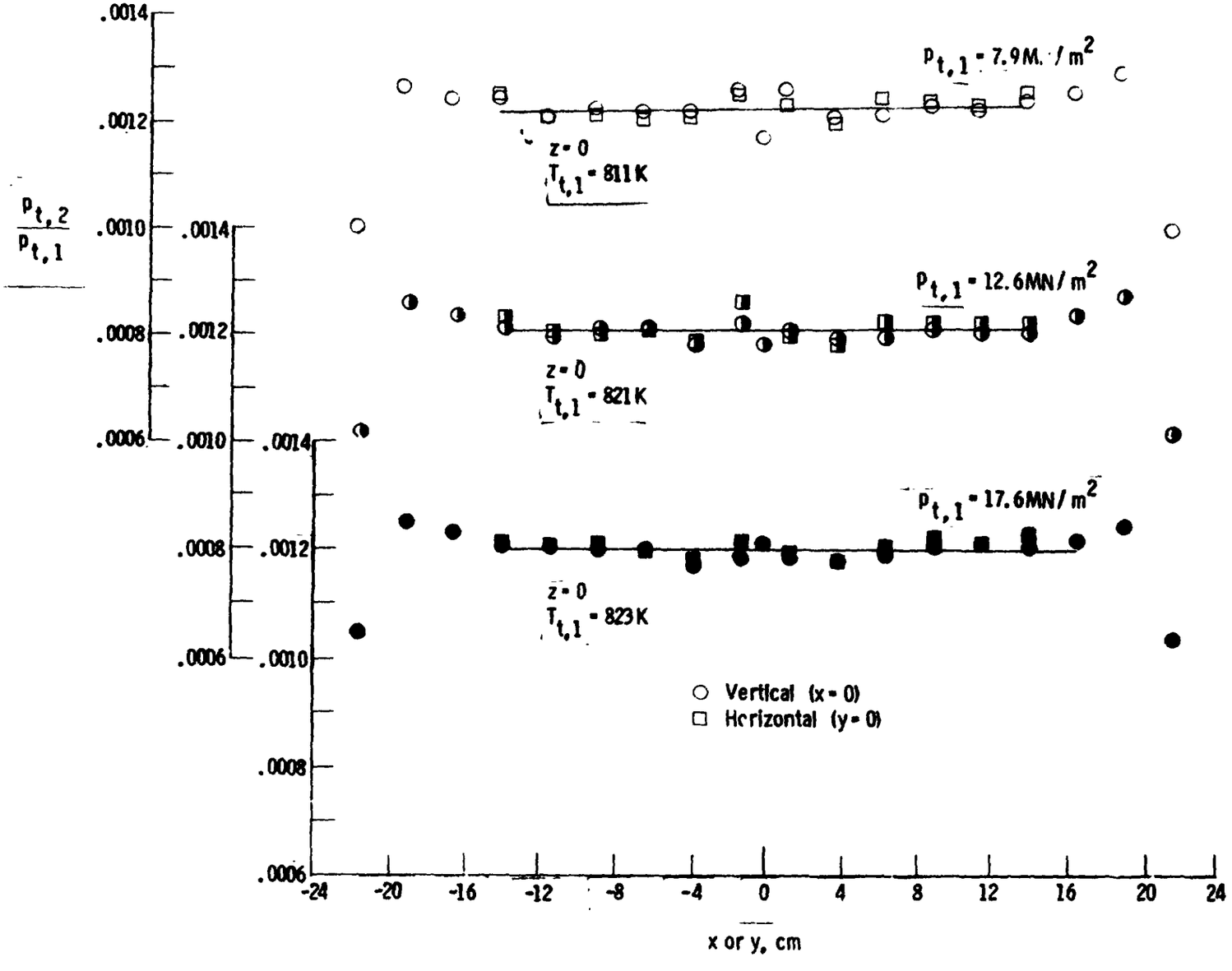

Figure 19. - Pitot pressure profiles at nozzle exit for $\bar{T}_{t,1} \approx 815$ K and various values of $p_{t,1}$.

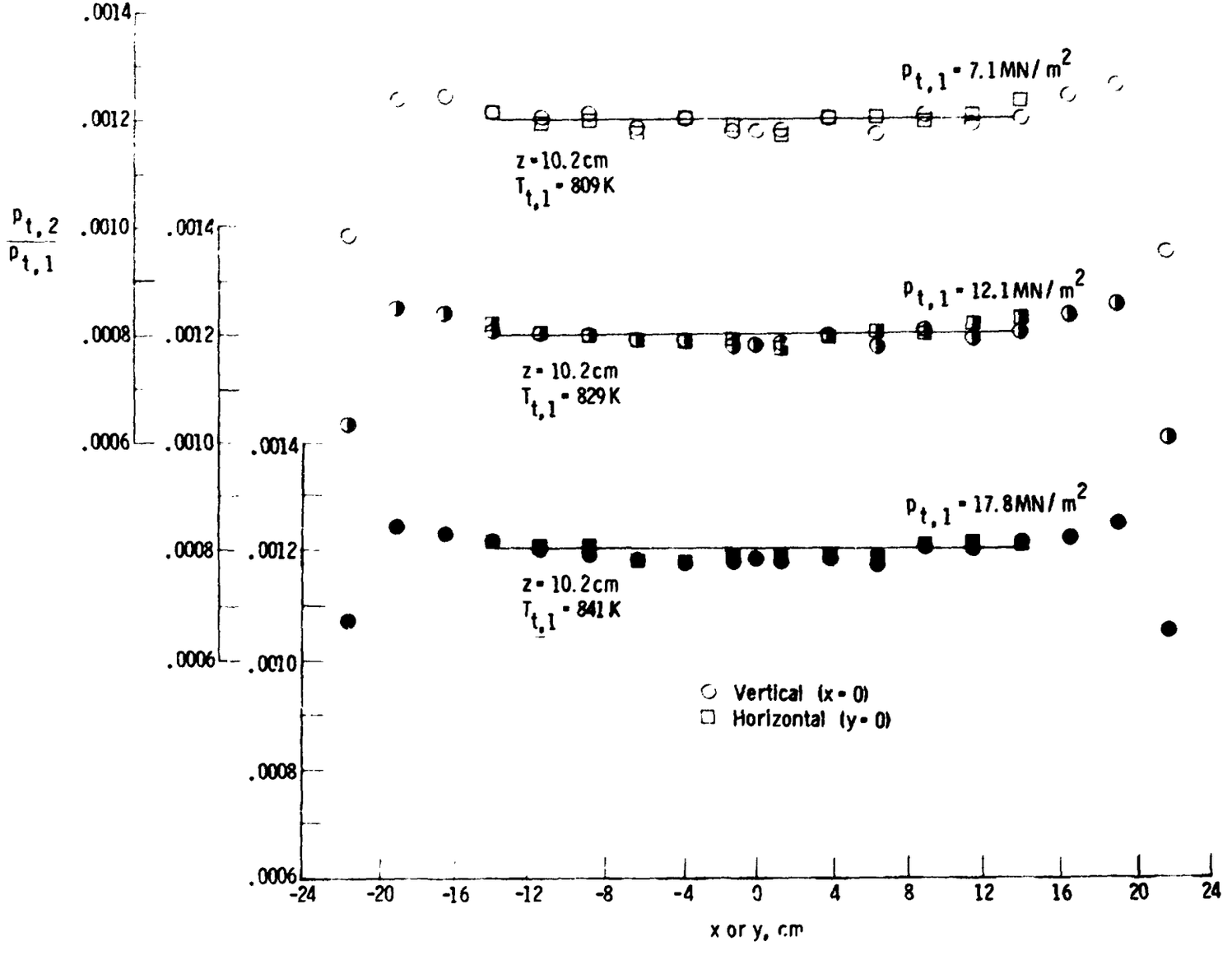

Figure 20. - Pitot pressure profiles 10.2cm downstream of the nozzle exit for $\overline{T}_{t,1} \approx 815$ K and various values of $p_{t,1}$.

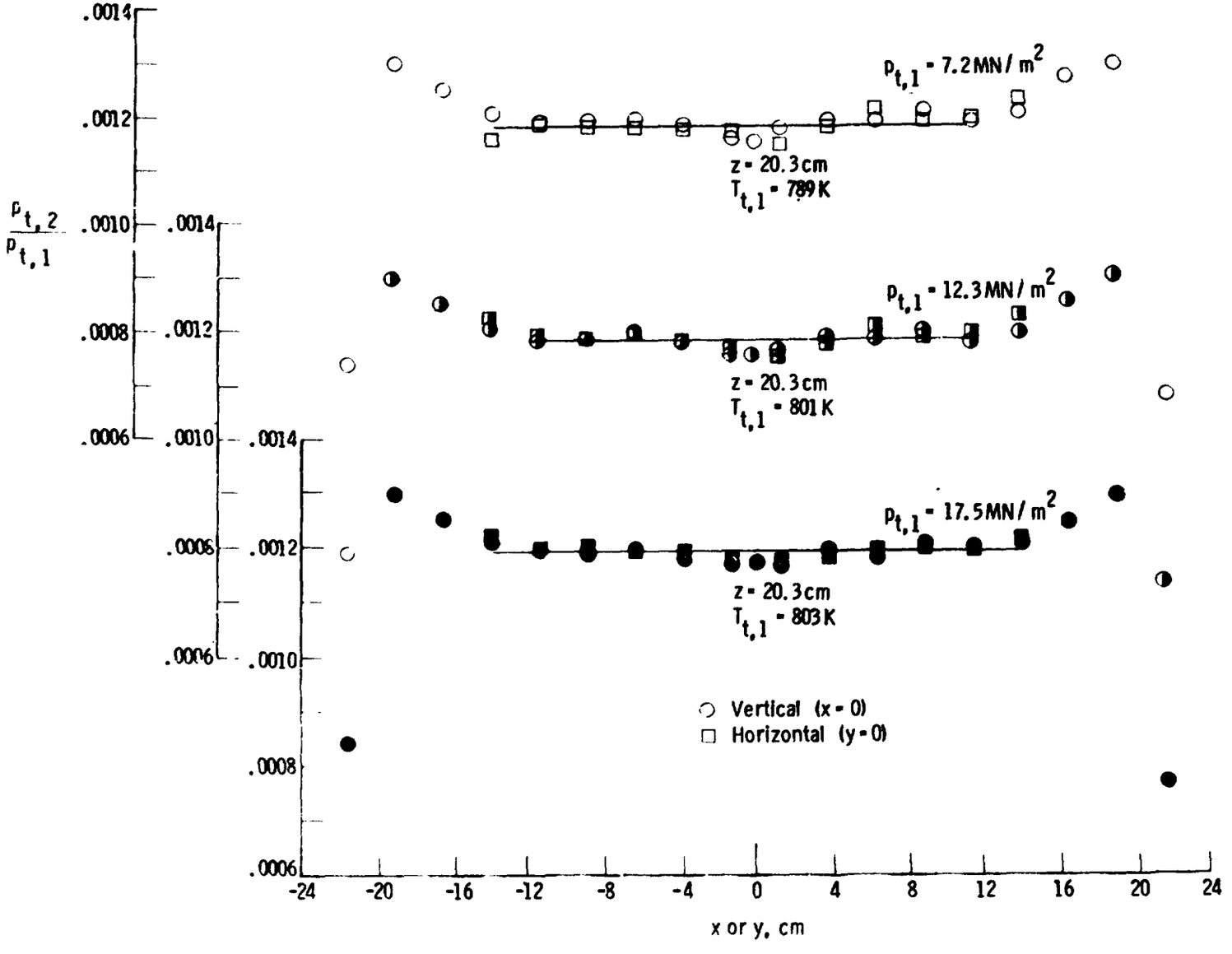

Figure 21. - Pitot pressure profiles 20.3cm downstream of the nozzle exit for $T_{t,1} \approx 815$ K and various values of $p_{t,1}$.

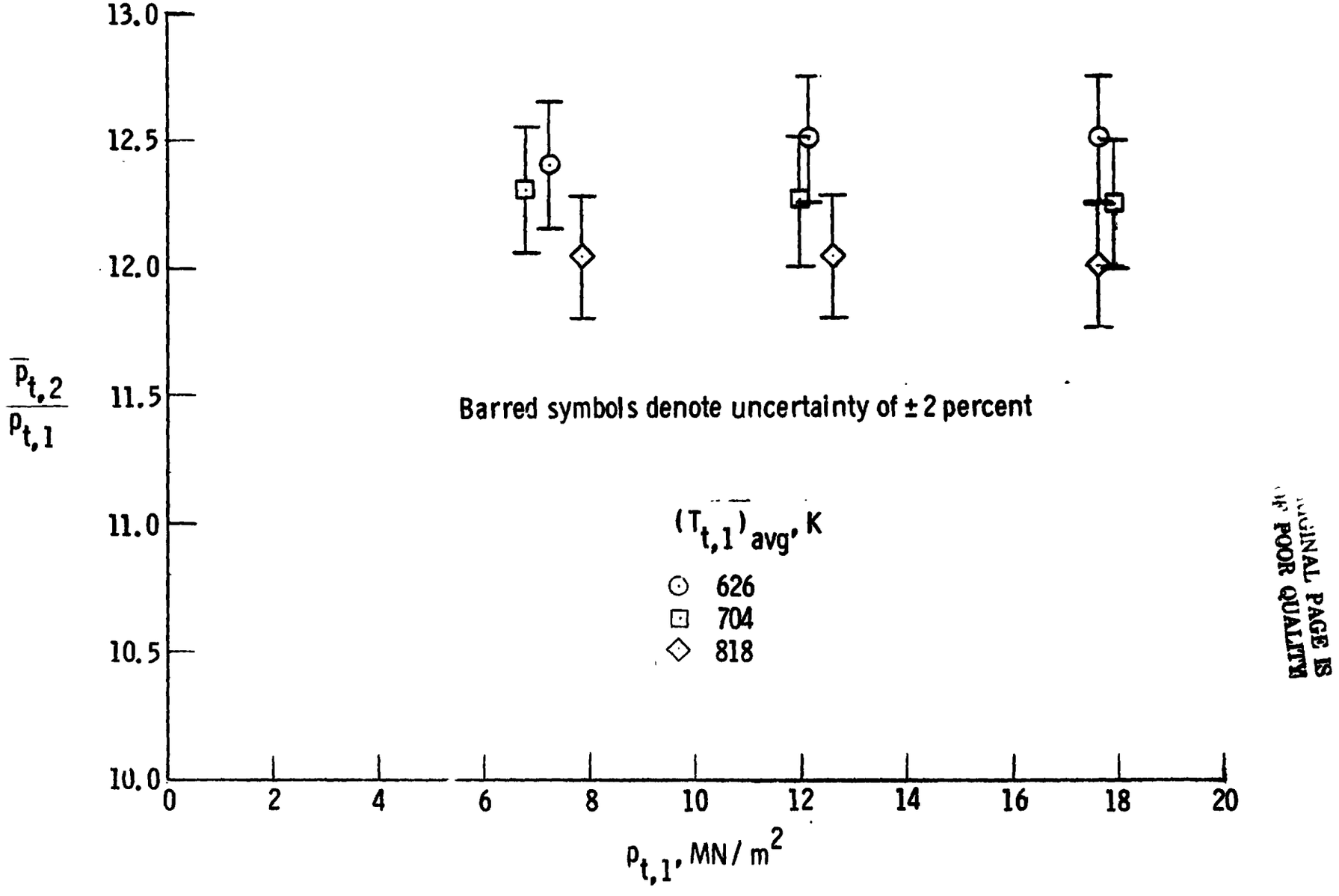

Figure 22. - Average pitot pressure ratio across inviscid test core as a function of stagnation pressure for several values of stagnation temperature.

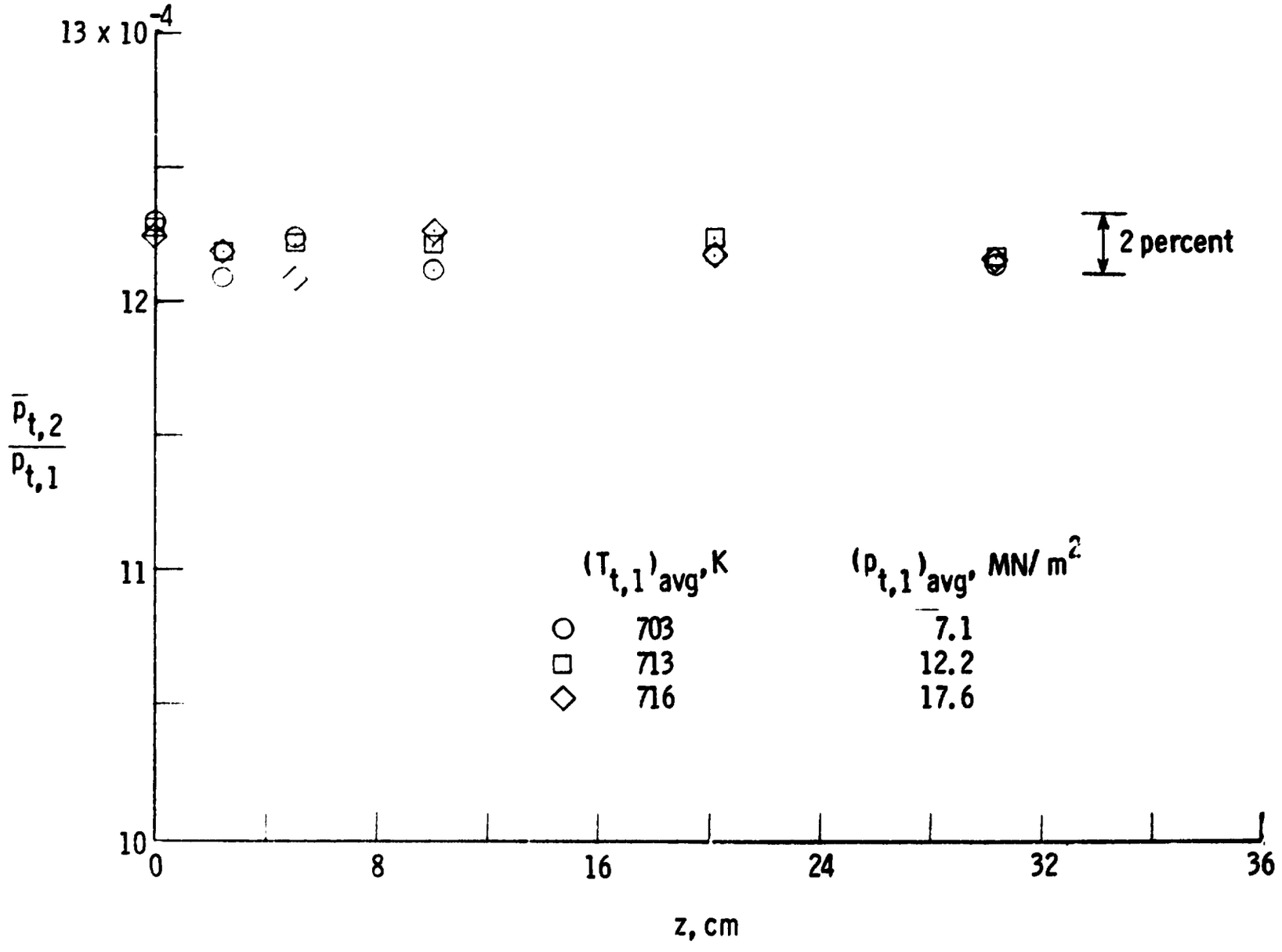

Figure 23. - Average pitot-pressure ratio across inviscid test core as a function of axial distance downstream of the nozzle exit for a nearly constant value of stagnation temperature.

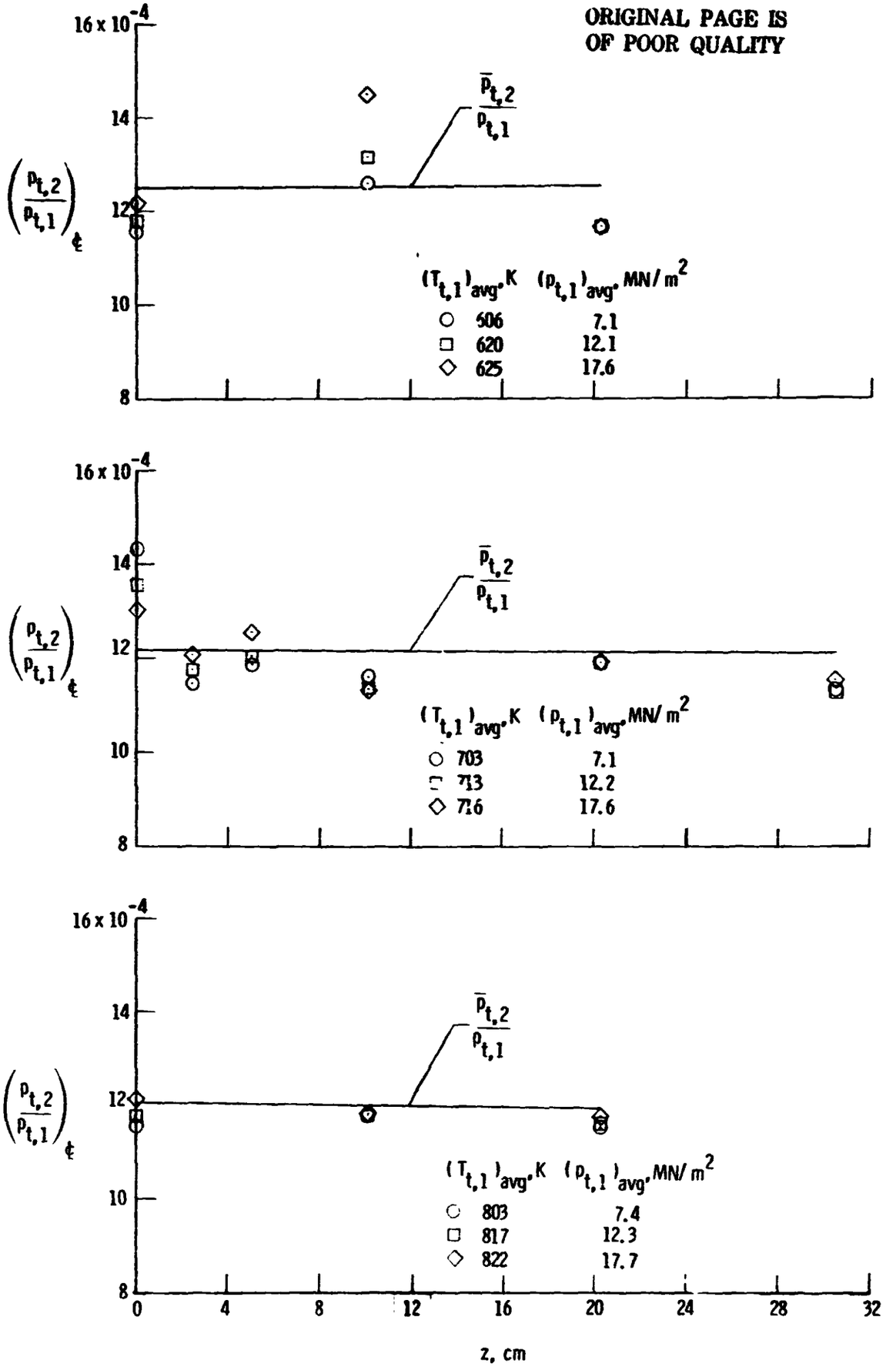

Figure 24. - Nozzle centerline pitot-pressure ratio as a function of axial distance downstream of nozzle exit.

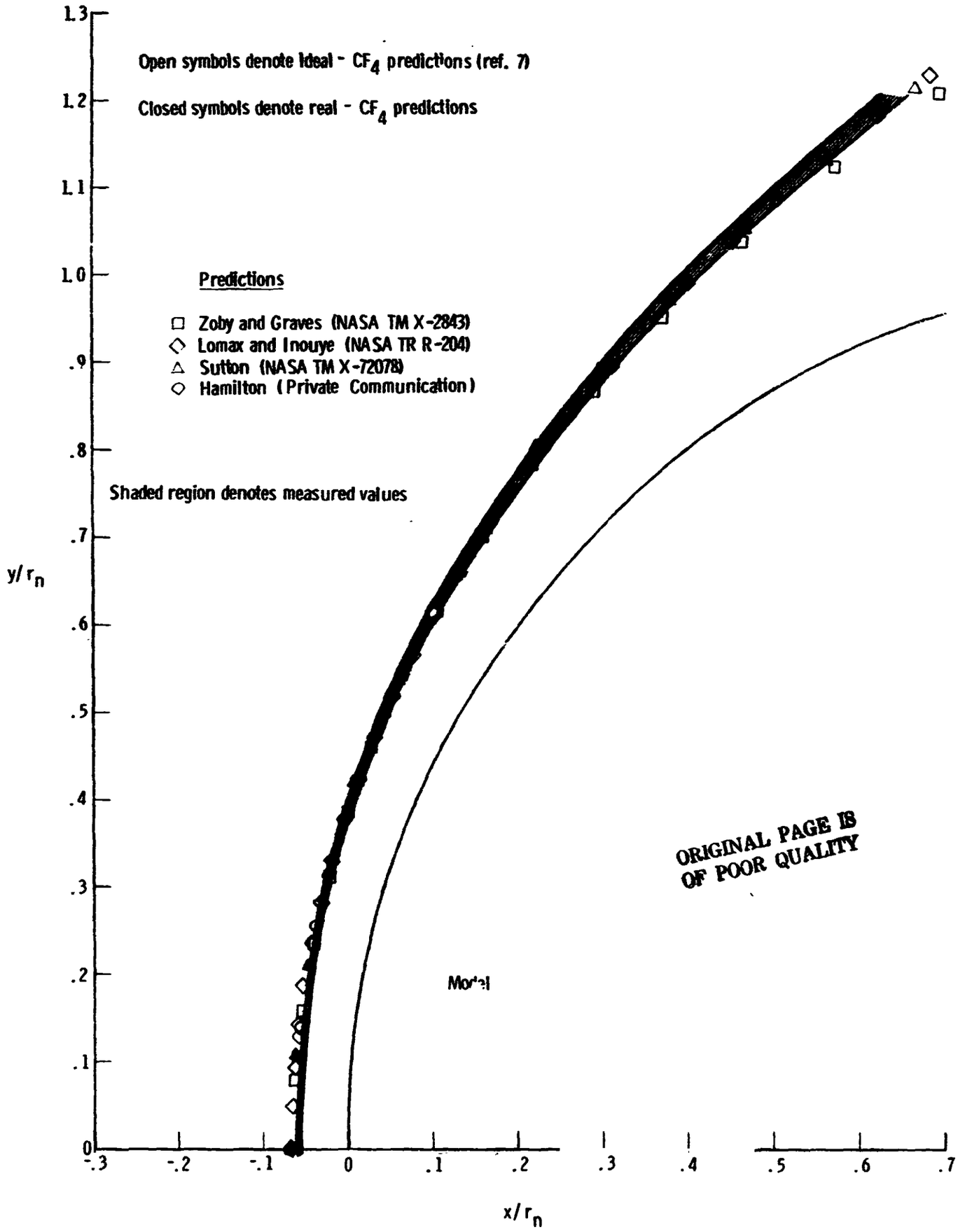

Figure 25. - Comparison of measured and predicted shock detachment distance for a sphere in Mach 6.15 CF_4 flow.

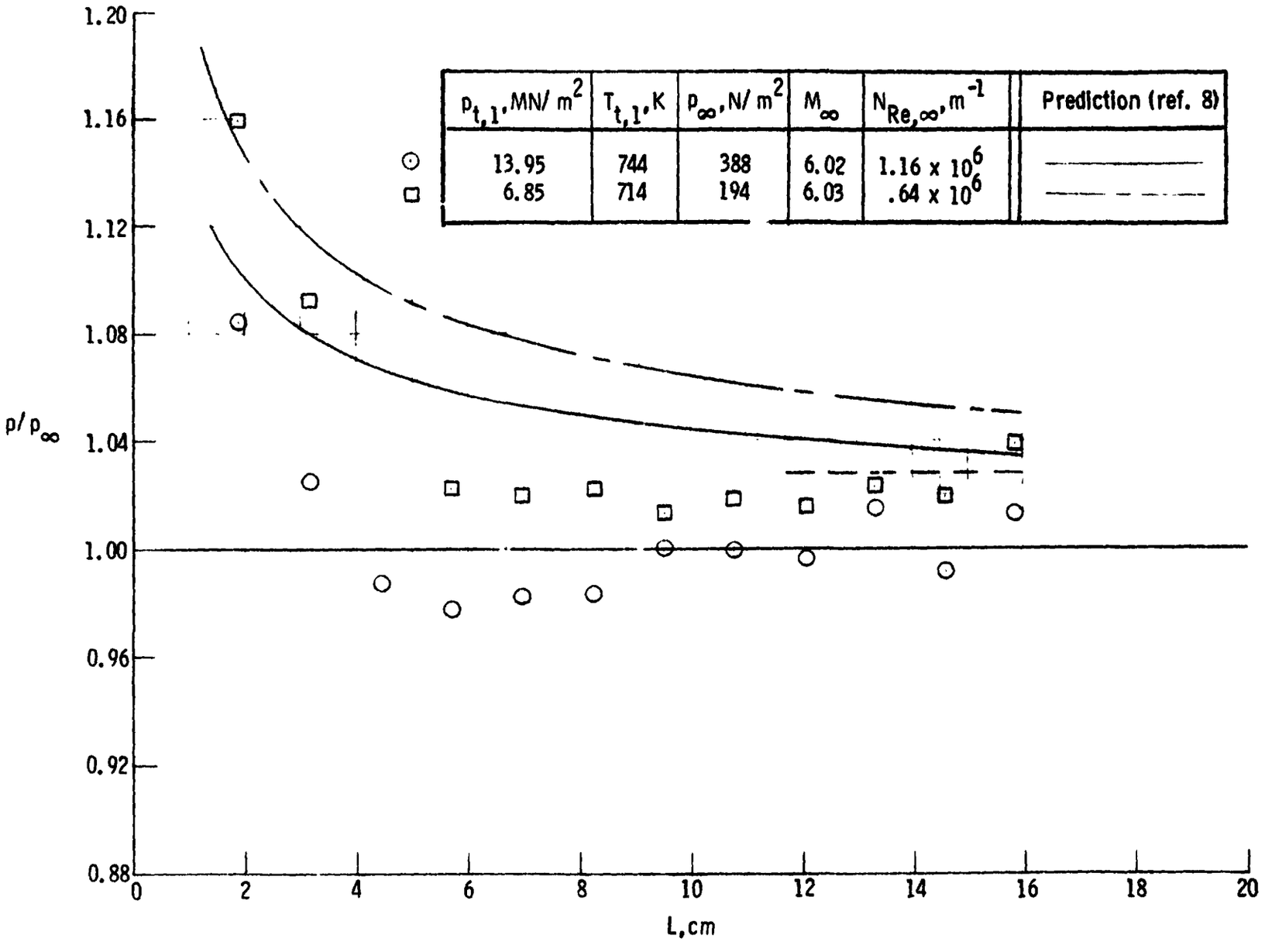

Figure 26. - Surface pressure distribution on center ray of sharp-leading-edge flat plate.

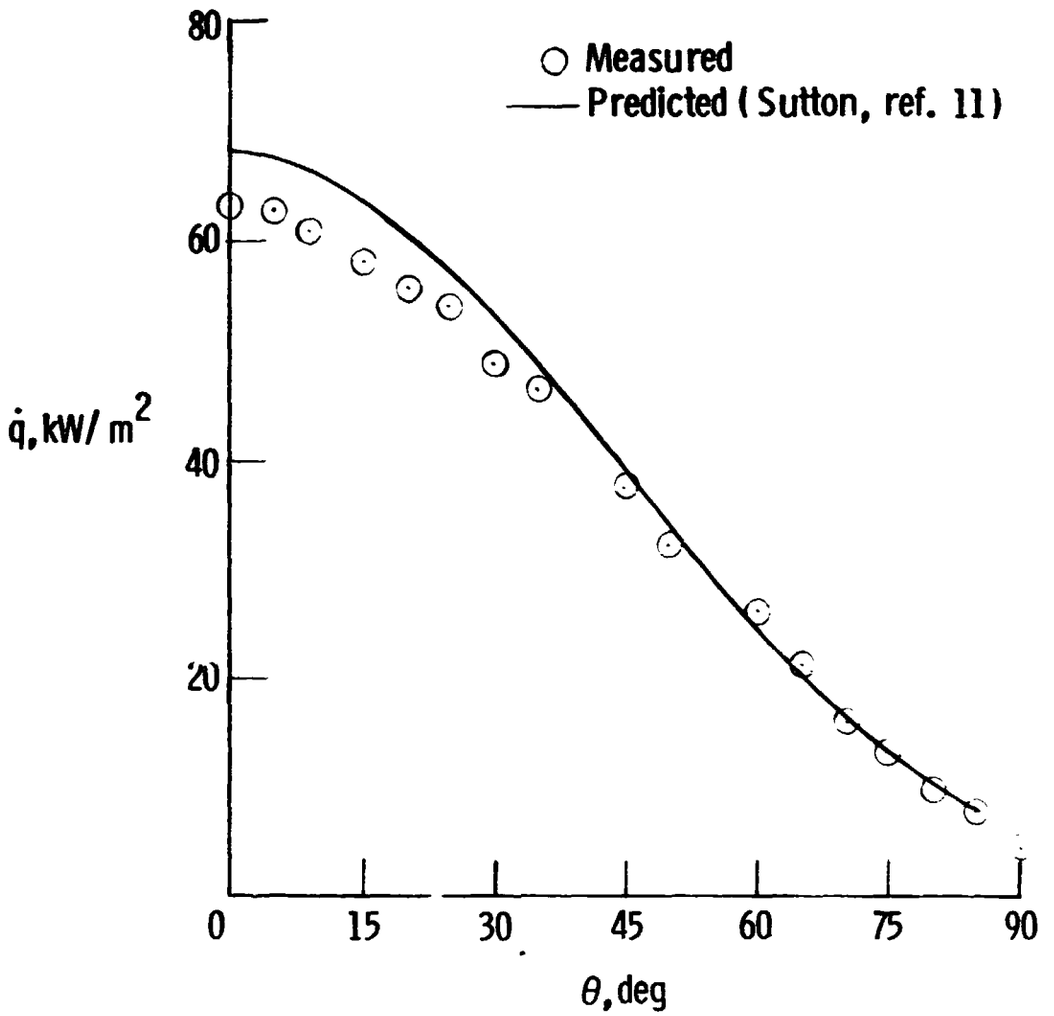

Figure 27. - Heat transfer distribution on 10.2 cm diameter hemisphere cylinder in Mach 6 CF_4 flow.